NORWEGIAN JOURNAL OF GEOLOGY
https://dx.doi.org/10.17850/njg103-2-4

GEOLOGICAL SOCIETY OF NORWAY

Gas seeps in Norwegian waters – distribution and mechanisms

Terje Thorsnes[1,2*], Shyam Chand[1,2], Valerie Bellec[1], F. Chantel Nixon[3], Harald Brunstad[4], Aave Lepland[1], Sigrun Melve Aarrestad[5]

[1]*Geological Survey of Norway (NGU), P.O. Box 6315 Torgarden, 7491 Trondheim, Norway*
[2]*CAGE – Centre for Arctic Gas Hydrate, Environment and Climate, Department of Geology, UiT the Arctic University of Norway, 9037 Tromsø, Norway*
[3]*Department of Geography, Norwegian University of Science and Technology, P.O. Box 8900, 7491 Trondheim, Norway*
[4]*Aker BP ASA, P.O. Box 65, NO-1324 Lysaker, Norway, Norway*
[5]*Vestland fylkeskommune, P.O. Box 7900, 5020 Bergen, Norway*

**E-mail corresponding author (Terje Thorsnes) terje.thorsnes@ngu.no*

Keywords:
- *Gas flares*
- *Cold seeps*
- *Carbonate crusts*
- *Methane seepage*
- *MAREANO*

Electronic supplement 1: Gas seeps

Received:
30. September 2022

Accepted:
2. May 2023

Published online:
1. June 2023

Gas seeps and fluid-flow related seabed features are found over the entire Norwegian exclusive economic zone (EEZ). Multibeam water-column data from *c.* 136 000 km² has revealed more than 5 000 gas seeps. Most of the gas seeps seem to have biogenic, thermogenic or mixed origin; some may be of abiotic origin. The spatial distribution of the gas seeps appears to correlate with: 1 – structural highs with associated faulting, exposing hydrocarbon reservoir rocks at or near the seabed; 2 – faults serving as conduits for fluid flow; 3 – settings where reservoir rocks overlain by less permeable cap rocks sub-crop at the seabed. Other mechanisms involve seepage around abandoned exploration wells, and possible abiotic gas generation from serpentinisation of ultramafic rocks near mid-oceanic ridges. The gas seeping from the Norwegian cold seeps is mostly methane and has, in many places, led to the formation of methane-derived authigenic carbonate crusts, which give evidence for either extensive gas seepage in the past or long-lived seepage. Chemosynthetic communities are commonly associated with cold seeps and may form special habitats together with the carbonate crusts. Methane seepage has been proposed to contribute significantly to the global carbon budget and may be associated with gas hydrates giving rise to potential geohazards. Gas seeps have been identified and spatially mapped as acoustic gas flares, using multibeam echosounder systems, which have the ability to record reflections from both the water column and the seabed. Water-column data have been recorded in the MAREANO seabed mapping program since 2010, covering an area of *c.* 262 000 km², with a data volume in the order of 210 Tb. The observations of extensive gas flares in the Norwegian EEZ are available to the scientific community and other users through a dedicated MAREANO data and web access system.

Thorsnes, T., Chand, S., Bellec, V., Nixon, F.C., Brunstad, H., Lepland, A., & Aarrestad, S.M. 2023: Gas seeps in Norwegian waters – distribution and mechanisms. *Norwegian Journal of Geology 103*, 202309. https://dx.doi.org/10.17850/njg103-2-4

Introduction

Marine methane vents and cold seeps are found on continental margins worldwide (Campbell, 2006; Skarke et al., 2014; Suess, 2014), releasing methane and supporting microbial bacterial communities (Orphan et al., 2004). Cold seeps have been proposed to bring large quantities of greenhouse gases from the deeper geosphere to the water column (Pohlman et al., 2011) and to the atmosphere with adverse effects on global-scale climate change. Active seepage on the continental shelf is commonly associated with underlying oil and gas reservoirs, trapped gas under gas hydrates, and the dissociation of gas hydrate itself (Milkov & Sassen, 2003; Pohlman et al., 2009; Sassen et al., 1999). Gas seeps can also be associated with hydrothermal vents at oceanic spreading centres, discharging fluids rich in CH_4 and H_2S (Campbell, 2006), with abiotic CH_4 from serpentinisation of ultramafic rocks (Charlou et al., 2010) or CO_2 emanating from submarine volcanic hydrothermal fields (Aiuppa et al., 2021).

It has been estimated that up to 10 000 Gt of methane carbon is associated globally with hydrate-bound gas (Milkov, 2004). Cold seeps are commonly associated with pockmarks (Hovland et al., 2002), but can also occur without forming pockmarks (Chand et al., 2012*a*). Cold seeps can give rise to methane-derived authigenic carbonate crusts, which are formed by anaerobic oxidation of methane (Greinert et al., 2001; Suess, 2014). Such crusts may form three-dimensional structures, creating rocky, cold-seep habitats, commonly associated with bacterial mats, obtaining their energy from the seeping methane (Aloisi et al., 2002; Chand et al., 2017; Åstrøm et al., 2018; Thorsnes et al., 2019).

The nature of the cold seeps varies significantly from one area to another, reflecting different mechanisms of fluid generation and tectonic or stratigraphic frameworks for creating fluid pathways (Naudts et al., 2010). The rate of gas flow over time may also vary considerably, likely in relation to external pressure changes, such as tides and changes in current directions (Naudts et al., 2010). Relative changes of up to an order of magnitude over time scales of hours have been suggested from the northern Gulf of Mexico (Jerram et al., 2015).

Numerous gas seeps in the water column have been identified along the Arctic shelf (Westbrook et al., 2008, 2009; Mau et al., 2017) and the northern US Atlantic margin (Skarke et al., 2014) and are thought to be associated with changes in gas hydrate stability conditions (Westbrook et al., 2008), discharges along major fracture zones (Mau et al., 2017) and focused fluid flow (Hustoft et al., 2009; Chand et al., 2012*a*).

Gas bubbles can be detected by several methods, such as visual identification using ROV (Remotely Operated Vehicles; Hovland 2002), or as acoustic signals, since gas bubbles give sufficient acoustic impedance contrast relative to seawater. Acoustic tools for detecting gas bubbles include subbottom profiler records and single-beam echosounder records (e.g., Naudts et al., 2006), sidescan sonar records (Uchimoto et al., 2019), and multibeam echosounder records (Greinert et al., 2006; Nikolovska et al., 2008). In this paper, we use the term 'gas flare' where acoustic data indicate a train of gas bubbles rising through the water column from a gas seepage site on the seafloor (Fig. 1). Other terms used in the literature include 'flares' (Schneider et al., 2007), 'hydroacoustic flares' (Jones et al., 2010), 'acoustic flares' (Mau et al. 2017), 'plumes of gas bubbles' (Westbrook et al., 2009) and 'water-column anomalies' (Skarke et al., 2014). The apparent strength of the flares depends on several factors, such as echosounder frequency and the size and physical properties of the bubbles (Jerram et al., 2015). Gas bubbles forming in the gas hydrate stability zone may have a hydrate coating on the bubble wall (McGinnis et al., 2006), reducing the rate of dissolution of methane in seawater. Gas seeps rising several hundreds of metres through the water column have been reported from the Gulf of Mexico (Weber et al., 2014), and seeps rising up to 1300 m have been observed in the Black Sea (Greinert et al., 2006).

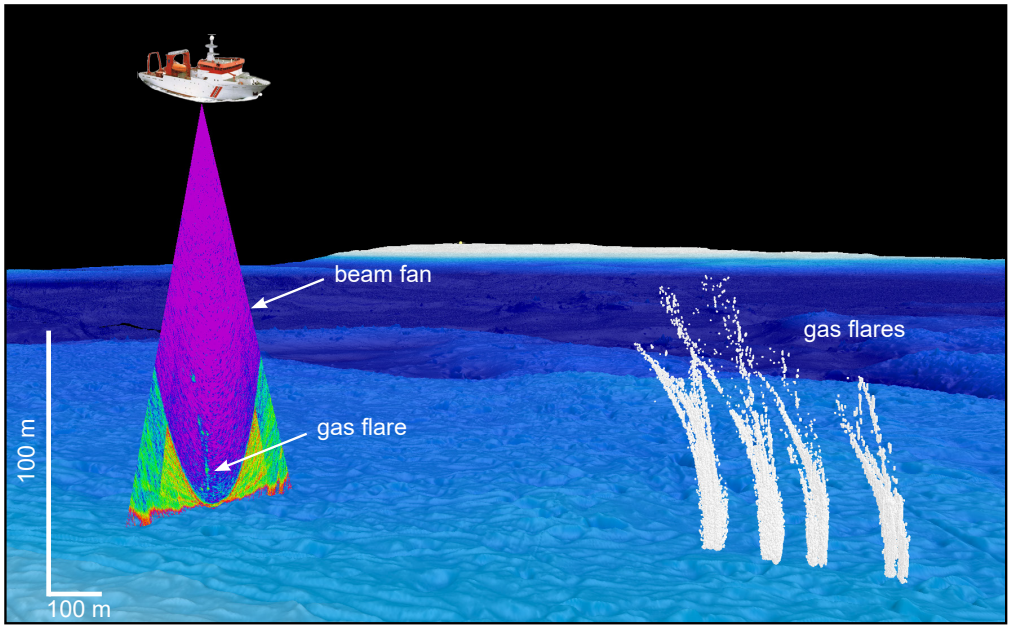

Figure 1. Visualisation of gas flares in the multibeam echosounder beam fan, showing records from the vessel H.U. Sverdrup II (Norwegian Defence Research Establishment) using a Kongsberg EM710 system in the Harstad Basin off northern Norway. 5x vertical exaggeration). The violet colour shows background noise.

The purpose of this paper is to provide an overview of the distribution of gas flares in Norwegian waters surveyed by the MAREANO program (Thorsnes et al., 2020) and point towards possible mechanisms for the seepage of gas. This overview can provide a framework for future scientific studies addressing fluid flow from subsurface to seabed, climate studies involving volumes of gas released to the ocean and atmosphere, and geohazard studies. The results will be published as a web service on www.mareano.no. The results shown in this paper are gas flares, where we have estimated the confidence for being a gas flare as 50% or higher. The web service will also include gas flares with lower confidence to allow users to investigate uncertain anomalies. The data will also be published as an electronic supplement (Electronic supplement 1).

Geological setting

The main study areas are the Norwegian Sea and Barents Sea shelves (Fig. 2). Analyses of multibeam data from the deepest parts of the Norwegian Sea, including the Arctic Mid-Ocean Ridge, are also included. The Barents Sea and the Norwegian Sea shelves are epicontinental, shallow sedimentary platforms, bounded to the west by the continent-ocean boundary (Gudlaugsson et al., 1998; Faleide et al., 2008). The Barents Sea comprises the Norwegian shelf in the west, the Russian shelf in the east, and extends northwards to the Hinlopen Margin, which separates the Barents Sea from the Arctic Ocean. The Norwegian part of the Barents Sea is underlain by the late Neoproterozoic–Cambrian Timanian basement, and reorganisation of it during the Caledonian and later orogenies (Gernigon et al., 2014; Klitzke et al., 2019). . The Norwegian Sea shelf is bounded towards the east by the Caledonian basement, and by oceanic crust of the Norwegian Sea to the west. Both the Barents Sea and the Norwegian Sea shelves have experienced several phases of extensional and contractional deformation since the Paleozoic, shown by a faulted and rugged basement (Faleide et. al., 2008). Several major rift phases have affected the Norwegian Sea shelf and the Barents Sea, and fault structures created during these episodes, and during contractional deformation may serve as conduits for fluids migrating from reservoirs.

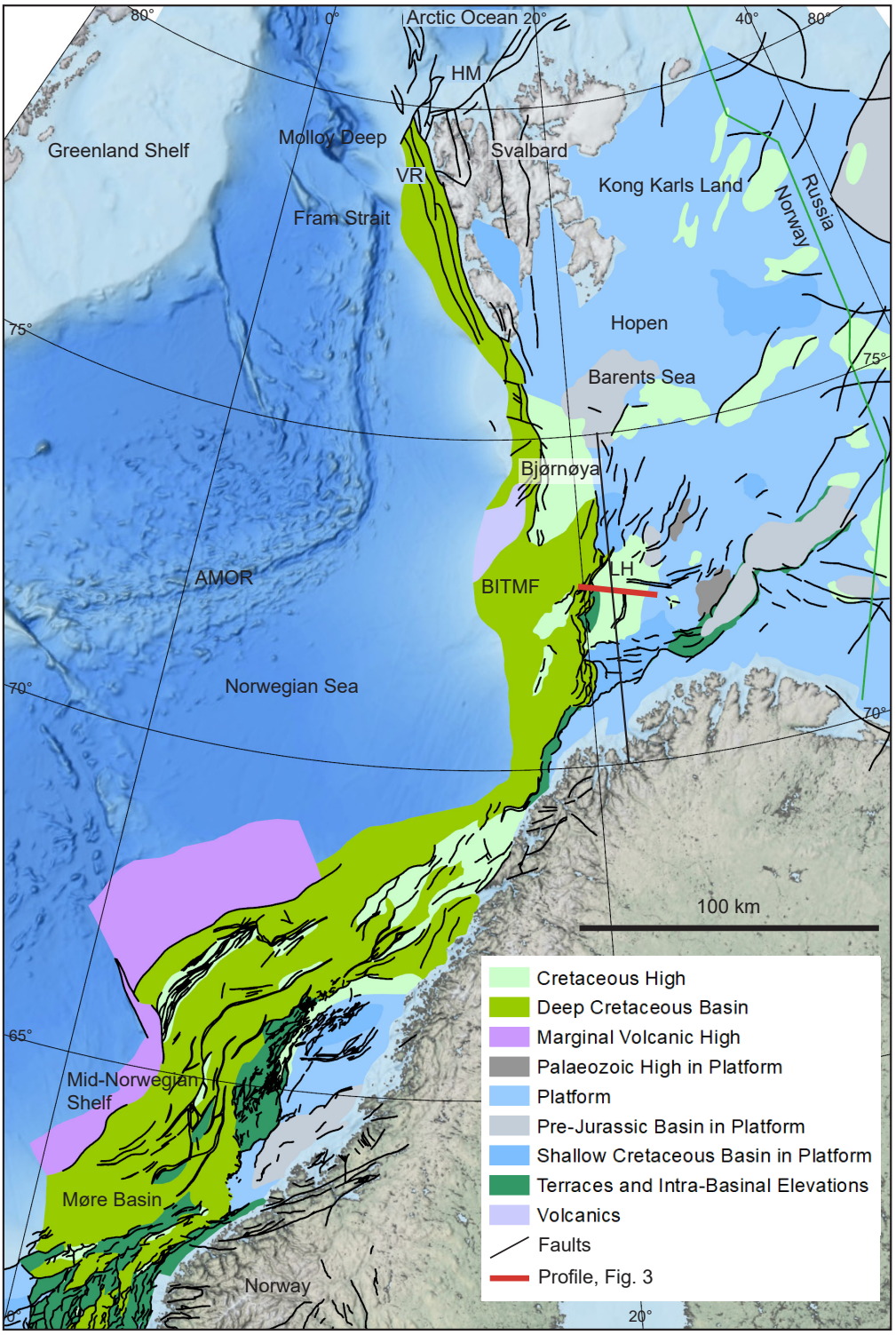

Figure 2. Structural elements of the Mid–Norwegian Shelf and the Barents Sea (NPD 2022). Source NPD 19.01.2022. AMOR – Arctic Mid-Ocean Ridge.

The Timanian and Caledonian orogenies, including the Devonian Svalbardian phase, formed the tectonic basement of most of the Norwegian Barents Sea Shelf (Gernigon et al., 2014; Klitzke et al., 2019) and the Mid Norwegian shelf (Blystad et al., 1995). The post-orogenic Devonian strike-slip to extensional regime generated small narrow basins filled with thick, steeply tilted sedimentary packages that were eroded during a post–Devonian regional peneplanation (Osmundsen et al., 2002; Brunstad and Rønnevik, 2022).

In the early Carboniferous (Mississippian), sediments were deposited in a regime of crustal extension and related trans-tensional wrenching, leading to the formation of half grabens that provided accommodation space for accumulation of syn-tectonic sedimentary growth packages and active volcanism. In the late Carboniferous (Pennsylvanian), there was a general relaxation interrupted by episodes of extensional tectonism, including crustal wrenching and readjustments (Brunstad and Rønnevik, 2022).

The Late Permian–Early Triassic rifting and extensional tectonism occurred in the Norwegian Sea, including the Western Barents Sea Margin (Müller et al., 2005; Faleide et al., 2008), and the Uralian Orogeny, with compressional tectonism, started along the eastern margin of the Barents Sea. The central Barents Sea experienced wrenching tectonism and several large-scale, low-relief domes and sag basins formed, probably as a remote effect of the Uralian compression (Müller et al., 2019) and the long-distance influence of the rifting in the west. In the Late Jurassic–Early Cretaceous the Norwegian Sea and Western Barents Sea went through an active rifting phase, leading to the formation of numerous fault-block structures. There are also some indications of Late Jurassic compression in the northeastern parts of the Barents Sea (Grogan et al., 1999). During the Late Cretaceous, rifting in the Western Barents Sea and the Norwegian Sea ceased; at the same time, the northern Barents Sea Margin was uplifted during rifting and opening of the Arctic Ocean. From the end of the Cretaceous and into the Paleocene active extensional tectonic movements with rifting occurred in the Norwegian Sea and along the Western Barents Sea Margin (Tsikalas et al., 2008; Petersen et al., 2016). In the Earliest Eocene the extension led into plate break-up and a period of igneous activity and volcanism (from magnetic Chron 24, e.g., Gaina, 2014), followed by plate drift which has continued to the present day. Late Cretaceous–Cenozoic contractional deformation produced several inverted structures, such as domes and folds, in the Barents Sea (Gabrielsen et al., 1997; Faleide et al., 2008). Paleogene Greenland Plate kinematics is the most likely candidate for explaining contractional structures (Gac et al., 2020). Along a transform zone extending from west of Spitsbergen and into the northwestern flank of the Barents Sea there was a component of tectonic strike-slip movements, local pull-apart basins and local trans-pressional zones (e.g., Lasabuda et al., 2021). In the Norwegian Sea and its margins there has been more continuous deposition and maximum sedimentary burial and maximum maturation of hydro-carbon sources occurring more or less until today. In most of the Barents Sea, the maximum burial and maturation of hydrocarbon sources was reached in the Late Eocene, interrupted by later uplift and erosional phases. In the westernmost parts, however, there has been almost continuous deposition up to the present interrupted by some uplift and erosion in the late Paleogene (Ryseth et al., 2003), and accordingly maximum burial seems to have been reached today.

Deposition of sediments with high TOC content occurred during several periods. The most important period is considered to be the Late Jurassic, when deposition of oil and gas-prone organic-rich muds and clays were deposited on most of the Norwegian, and also the west European, shelves. In the Barents Sea these are named the Hekkingen Formation and on the Norwegian Sea shelf, the Spekk Formation (Dalland et al., 1998). On the Barents Sea Shelf , other organic-rich sediments include the Early–Middle Triassic organic-rich phosphatic shales (Botneheia and Steinkobbe formations), which were deposited in a deep shelf environment in the Barents Sea (Riis et al., 2008; Lundschien et al., 2014). Other possible source rocks in the Barents Sea, which vary in age from Middle Devonian to Early Cretaceous, have been reported (Henriksen et al., 2011). Modelling indicates that the methane source for extensive gas seeps offshore western Svalbard at the Vestnesa Ridge are Miocene sedimentary rocks (Knies et al., 2018). The formation of hydrocarbon traps and migration routes are the result of several important phases of active tectonism and structural shaping/reshaping. Elevated methane levels were found in seawater on the southwestern Spitsbergen shelf and have been attributed to submarine methane discharge from the seabed (Damm et al., 2005). More than 1000 active plumes have previously been described from the seabed along the West Spitsbergen margin (Westbrook et al., 2009; Mau et al., 2017). Studies on the shallow gas distribution and seafloor seepage in Nordfjorden (a tributary to Isfjorden) show that

methane seepage is important also in the fjords (Roy et al., 2019). Modelling of the gas hydrate stability zone in Svalbard's fjords indicates that natural gas hydrate occurrence is likely in many of the fjords, based on the presence of proven source rocks and active petroleum systems (Betlem et al., 2021).

The Loppa High (Fig. 3) provides a good case for demonstrating the complex interaction between deposition, maturation, migration and tectonic processes, facilitating fluid flow to the seabed (Brunstad & Rønnevik, 2022). The Loppa High with its flanks has been penetrated by a large number of wells, and these have proven the presence of sediments spanning much of the Carboniferous to Paleocene stratigraphic interval, including several major stratigraphic breaks. This gives a good fundament for understanding factors such as changes in sedimentary environments, paleoclimatology, periods with uplift and active tectonism, as well as source-rock development and potential hydrocarbon generation. Since the Loppa High with its flanks contains most of the relevant petroleum exploration plays of the Norwegian Barents Sea, this province has been much used by the oil companies as a laboratory for understanding the geology in other areas (Brunstad & Rønnevik, 2022).

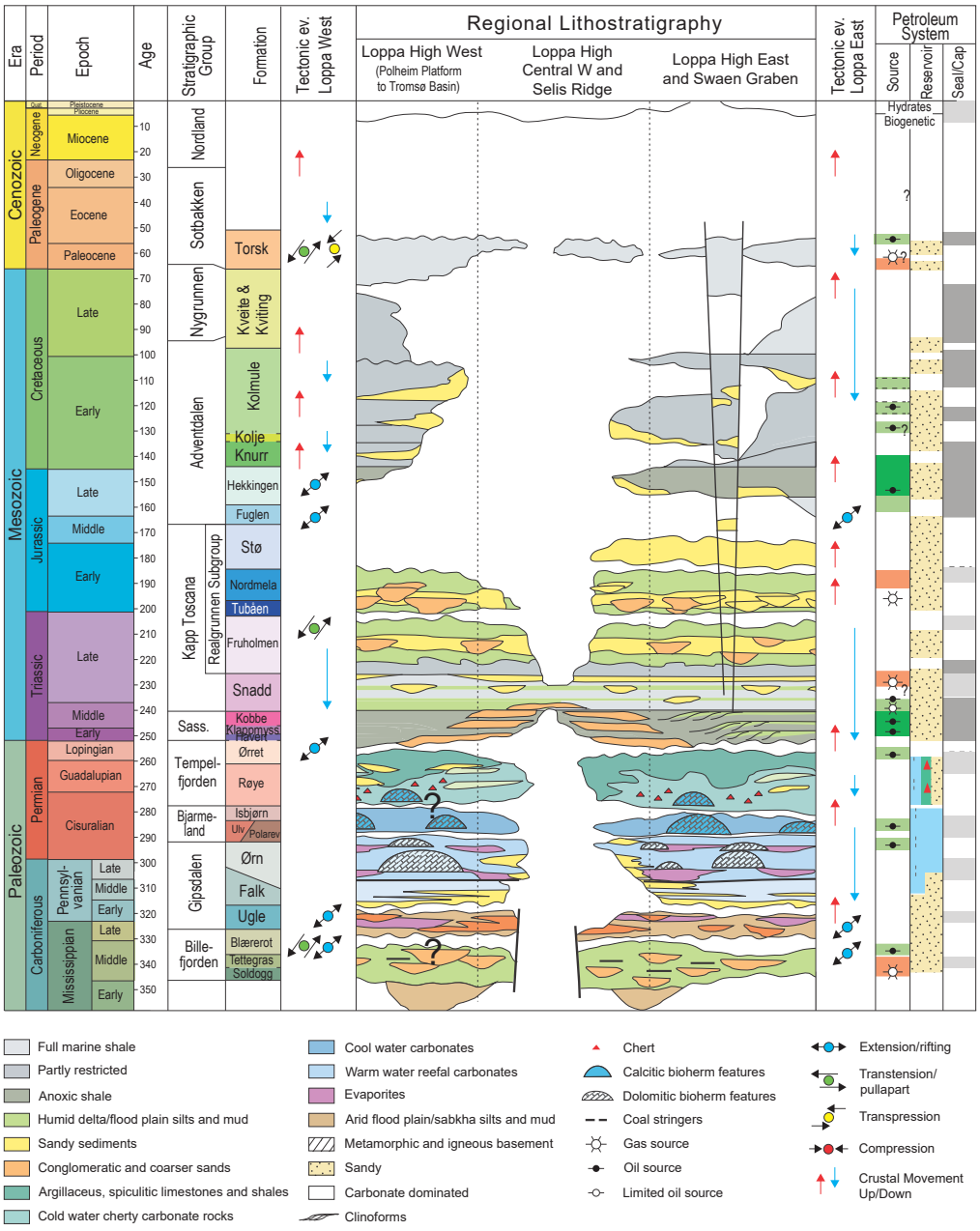

Figure 3. Stratigraphic log from the Loppa High, illustrating the complex interplay between deposition, maturation, potential source rocks, migration and tectonic processes. Modified from Brunstad & Rønnevik, 2022.

During the Mid–Pliocene to Early Pleistocene, the Barents Sea and adjacent land areas were uplifted (Vorren et al., 1991; Eidvin et al., 1993), and repeated glaciations have occurred during the Late Cenozoic (Vorren et al., 1989, 1998; Andreassen et al., 2008). During the Late Pliocene and the Pleistocene, average erosion of the southwestern Barents Sea was about 600 m (Henriksen et al., 2011). Glacial erosion was more severe in the southeastern parts compared to the west and north, and more extensive where former glacial ice streams formed (Eidvin et al., 1993). Close to 3 km of rocks have been eroded in the Svalbard area (Henriksen et al., 2011) since the Oligocene which is considered to be due mainly to the Paleogene tectonic uplift (Vorren et al., 1991; Eidvin et al., 1993).

An upper regional unconformity (URU) separates variously dipping sedimentary strata from the overlying upper horizontal glacigenic sequences (Vorren et al., 1989). Sediment sequences of varying thicknesses overlie the unconformity, with thicknesses between 0 and 300 m on the shelf proper, and 900–1000 m thickness at the continental margin (Vorren et al., 1989). Sediments up to more than 1000 m thick in the 'North Sea Fan' system going into the Møre Basin area, and more than 3000 m in the Bear Island Trough Mouth Fan (Laberg & Vorren, 1995) were deposited during the last 2.5–3.0 million years.

Gas hydrate stability studies have shown that gas hydrates, which are ice-like solid compounds of gas (mostly methane; Kvenvolden, 1988) and water, are stable over large parts of the Barents Sea (Chand et al., 2008; Andreassen et al., 2017; Betlem et al., 2021). Multiple episodes of fluid flow, evidenced by pockmarks, gas flares and gas hydrate accumulations, have occurred in the Barents Sea (Chand et al., 2012*a*, *b*; Andreassen et al., 2017). A study of 14 carbonate crusts from the northeastern part of the Norwegian Sea and the southwestern part of the Barents Sea (Crémière et al., 2016) has shown that the onset of methane release started at the same time as deglaciation-induced pressure release and thinning of the hydrate stability zone at 16–18 ka BP. Clustering of the U–Th dates from the crusts indicate that the main crust-forming methane flux episode took place between 17 and 7 ka BP. Massive blow-out craters and pingos formed by hydrate-controlled methane expulsion have been documented from several areas (Andreassen et al., 2017; Nixon et al., 2019). Geological controls of gas seepage at the seafloor in the Barents Sea have been suggested to be faults offsetting reservoirs/closures which continue up to the seafloor, areas where reservoir and cap rocks subcrop at the seafloor, and at the crests of large geological structures where Triassic or Jurassic reservoirs have been exposed due to erosion of the cap-rocks (Andreassen et al., 2017; Mattingsdal, 2020; Waage et al., 2020; Serov et al., 2023).

Vestnesa is a contourite drift ridge west of northern Spitsbergen, deposited during the Late Miocene and the Pliocene (Eiken & Hinz, 1993), that hosts gas hydrates and free gas. Numerous gas seeps and large pockmarks have been described from the crest of Vestnesa (Hustoft et al., 2009). Modelling from hydrate-modulated methane seepage suggests that continuous leakage from the seafloor has occurred since the Early Pleistocene until today, from deep subsurface thermogenic sources of Miocene age (Knies et al., 2018). Abiotic methane from high-temperature serpentinisation of ultramafic rocks in ultraslow-spreading ridges has been suggested to be an important source of methane in the Vestnesa Ridge area, where gas hydrate related anomalies have been observed on seismic data (Johnson et al., 2015). However, this was not supported by Panieri et al. (2017) who reported that the gas from the Vestnesa system has both microbial and thermogenic gas sources, with a predominantly mixed gas signature of methane in both of the sampled pockmarks (Lomvi and Lunde).

The Arctic Mid-Ocean Ridge (AMOR) extends from the northern shelf of Iceland through the Fram Strait, across the Eurasia Basin to the Siberian shelf in the Laptev Sea. The Molloy Deep is in the Fram Strait between Spitsbergen and Greenland (Fig. 2), and forms part of the AMOR which is an ultraslow spreading ridge, with widespread hydrothermal activity (Pedersen et al., 2010). The Molloy Deep

and the Molloy Ridge were formed 30–40 Ma ago with the opening of the Norwegian–Greenland Sea (Engen et al., 2003). In this region, the crust is thin, and the Moho is shallow (<5 km) (Czuba et al., 2005). The Molloy Deep represents a modern and evolving pull-apart basin. It occurs where the Atlantic Mid-Ocean Ridge has an offset, which created a transform boundary where the southern part of the transform fault is deeper than the northern part due to the relative movements between the ridge segments.

Materials and methods

In this study, multibeam echosounder data collected by the MAREANO seabed mapping programme (www.mareano.no), covering an area of c. 288 750 km² and collected between 2005 and 2021, were used to identify evidence for gas flares and fluid flow at the seabed. Since 2010, water-column data have been acquired from an area of c. 262 000 km2 in 621 surveys. To date, *c.* 137 000 km² from 321 surveys have been analysed for gas flares (Fig. 4 A & B).

The surveys were undertaken by commercial vendors, the Norwegian Defence Research Establishment (FFI), and the Norwegian Hydrographic Service using Kongsberg Maritime EM710, EM712, EM122, EM304 and/or EM2040 multibeam echosounder systems (Table 1). The EM2040, EM710 and EM712 were used in shallow to intermediate water depths. In deep waters, EM122 (12 kHz), has been used down to 2500 m water depth west of Spitsbergen, and an EM304 system was used for the deep parts of the Norwegian Sea, including the Arctic Mid-Ocean Ridge and the Molloy Deep.

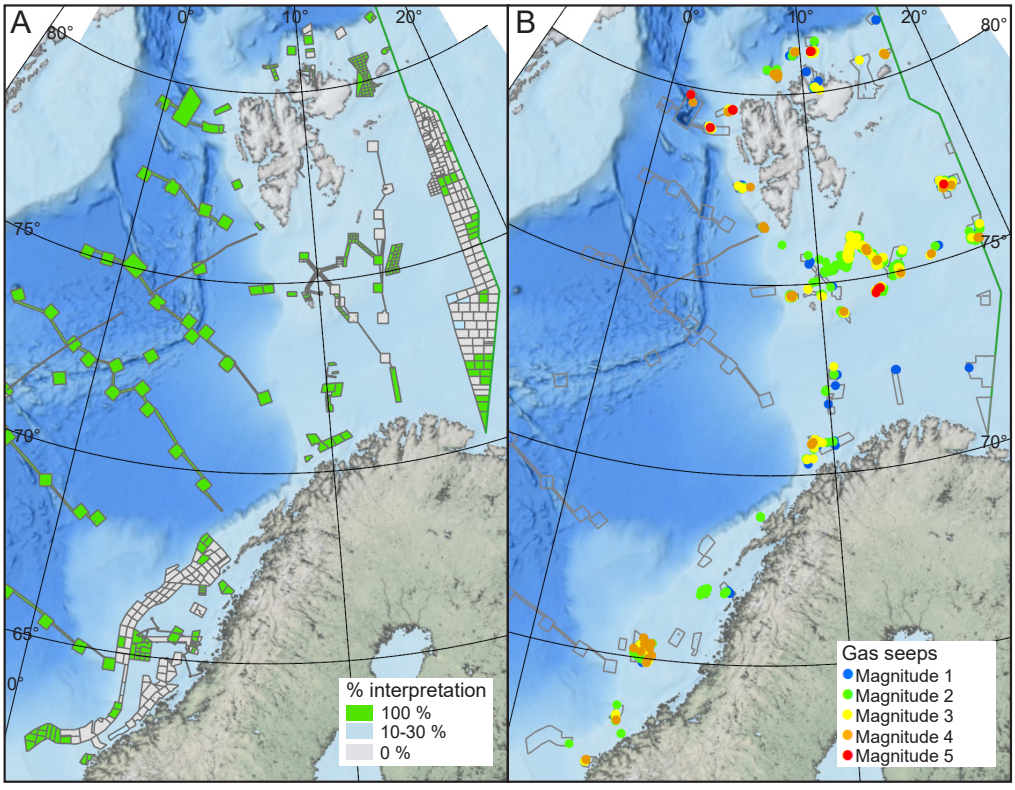

Figure 4. (A) Multibeam echosounder data with water-column data. (B) Interpreted gas flares.

Table 1. Kongsberg Maritime multibeam echosounder systems.

KM MBES system	Frequency, kHz	Maximum water depth (m)
EM122	12	Full ocean depth
EM304	20 – 32	11000
EM710	70 – 100	3000
EM712	40 - 100	3500
EM2040	200 - 400	600

The water-column data were stored in separate raw files (WCD files) in the Kongsberg system with a typical size of 0.8 Tb pr. 1000 km^2. The files are *c*. 5–20 times larger than the bathymetry raw files (ALL files), depending on water depth and system. The water-column data consists of several hundred beams with individual pings. As the ship moves forward, a 3D volume of the water column is generated (Fig. 1). This volume does not give hundred percent coverage of the water column since the overlap between the adjacent lines is often only up to 10% at the seafloor. The coverage of the beam fan increases with distance from ship and therefore we have a large gap in the data in the top part of the water column between adjacent lines. This could result in only a partial mapping of the water column and thereby missing some of the flares which occur in this grey zone.

The water-column raw data are stored in a dedicated database at the Norwegian Hydrographic Service. Analysis of the water-column raw data has been conducted by the Geological Survey of Norway. A Fledermaus Midwater (FMMW) package was used to process water-column data for detecting and analysing acoustic anomalies. The water-column raw data (WCD) were loaded in FMMW and combined with navigation from bathymetry raw data (ALL) and converted to Generic Water Column data (GWC) files.

Similar water-column anomalies detected in other areas of the Barents Sea have been ground-truthed, confirming the presence of gas seeps, and thus the feasibility of this method (Chand et al., 2012a, *b*, 2016; Chand & Thorsnes, 2020). During interpretation, the following procedure was followed as far as possible:

1. The depth range was adjusted to maximise the vertical display of the line (FMMW).
2. The display was adjusted to 1:1 horizontal display (FMMW).
3. The colour range was adjusted to the dynamic range of signals in the water column, optimising the display of water-column features (FMMW). Here, we used different ranges based on the system and general loss in the water column through visual inspection. The range is kept constant for the whole survey to avoid any inconsistency related issues.
4. The data were inspected using the R-stack water column view, and the stacked-fan water column view. The R-stack mode takes all of the beams in the swath, collapses them down together in an over lapped manner and displays the maximum signal level for every discrete range increment in the display.
5. The locations of gas flares were determined using the GeoPick function in FMMW.

The water-column data were evaluated in parallel (R-stack along-track, left panel) and perpendicular (Fan view, across-track, right panel) directions to the track lines for identifying anomalies (Fig. 5). All of the examples shown in Fig. 5 display straight vertical noise patterns, which may obscure the gas flares. This is particularly noticeable for the example for M4. More examples of noise are found in Fig. 6. The coordinates, time of acquisition, water depth, and height of gas flares were recorded,

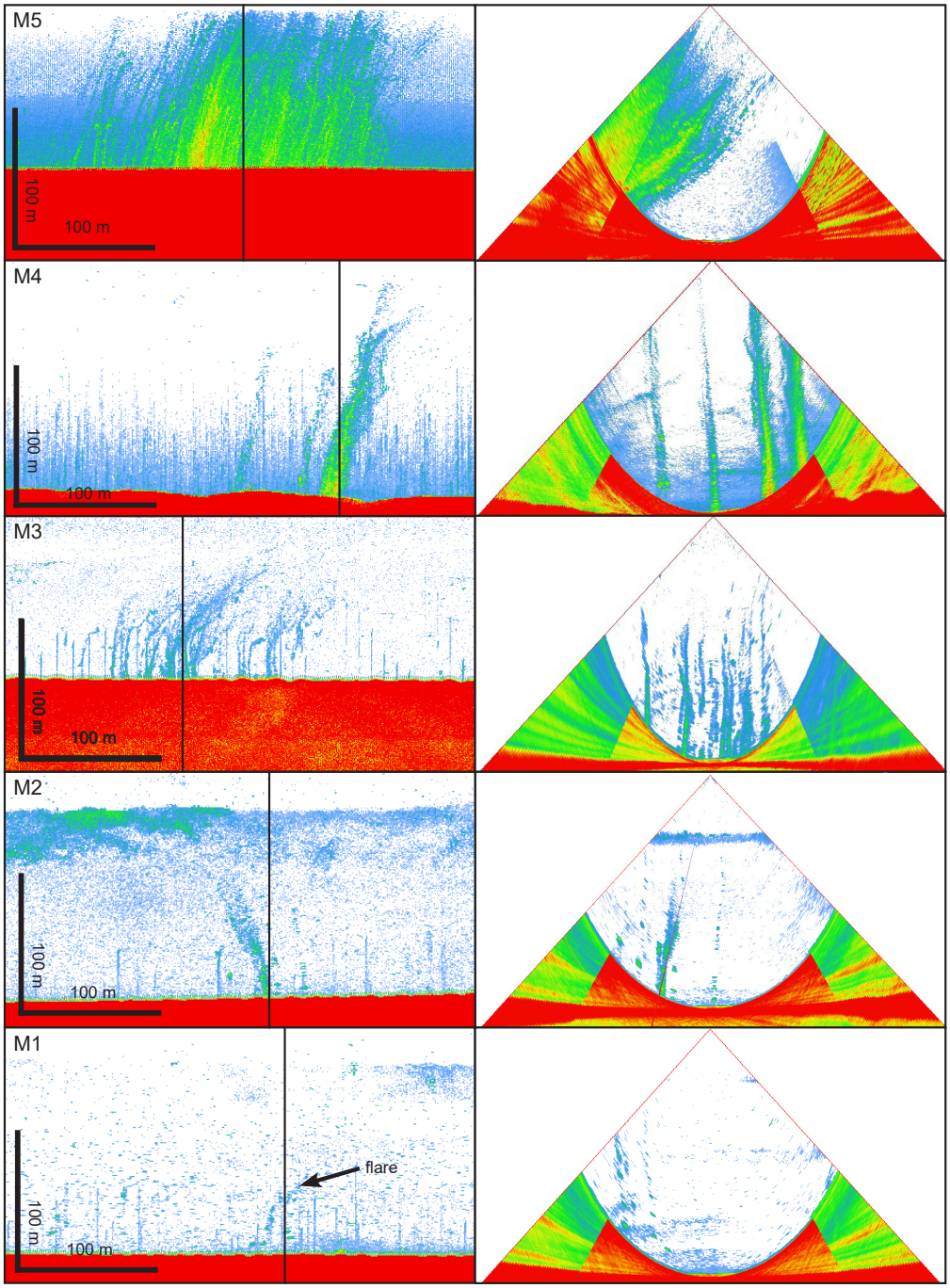

Figure 5. Examples of gas flares, with magnitude 1–5. Left column: gas flares identified along the track lines. Black line shows position of the section in the right column. Right column: gas flares identified in the beam fan (perpendicular to track line).

along with the survey name and line ID. The position error of the determined location is estimated to 5% of the water depth or less, based on seep locations determined from water-column data which have been ground-truthed by ROV surveys (Thorsnes et al., 2019). A subjective assessment of the apparent magnitude has been assigned (Table 2). A confidence estimate is provided based on an expert assessment. The maximum confidence for visual classification is 90%. A confidence of 100% is reserved for gas flares where gas bubbles have been observed by video/photo inspection or measured using gas sniffers, or where authigenic carbonate crusts have been observed, or where microbial mats have been observed. Acoustic anomalies which may be gas flares or may have an uncertain or very uncertain origin have been assigned 40–10% confidence.

Besides the migration of free gas from biogenesis and direct gas migration from a petroleum kitchen or reservoir, oil in the subsurface generally contains gas, which is often termed 'associated gas'. Upon oil migration towards shallower strata and the seabed, the gas is gradually released. This release also happens in the water column and is likely to be visible in the water column data. Moreover, whereas methane is generally dissolved in water before reaching the sea surface, the oil droplets should be expected to bleed off gas all the way to the sea surface. As such, gas from oil seeps is expected to have greater visibility throughout much of the water column.

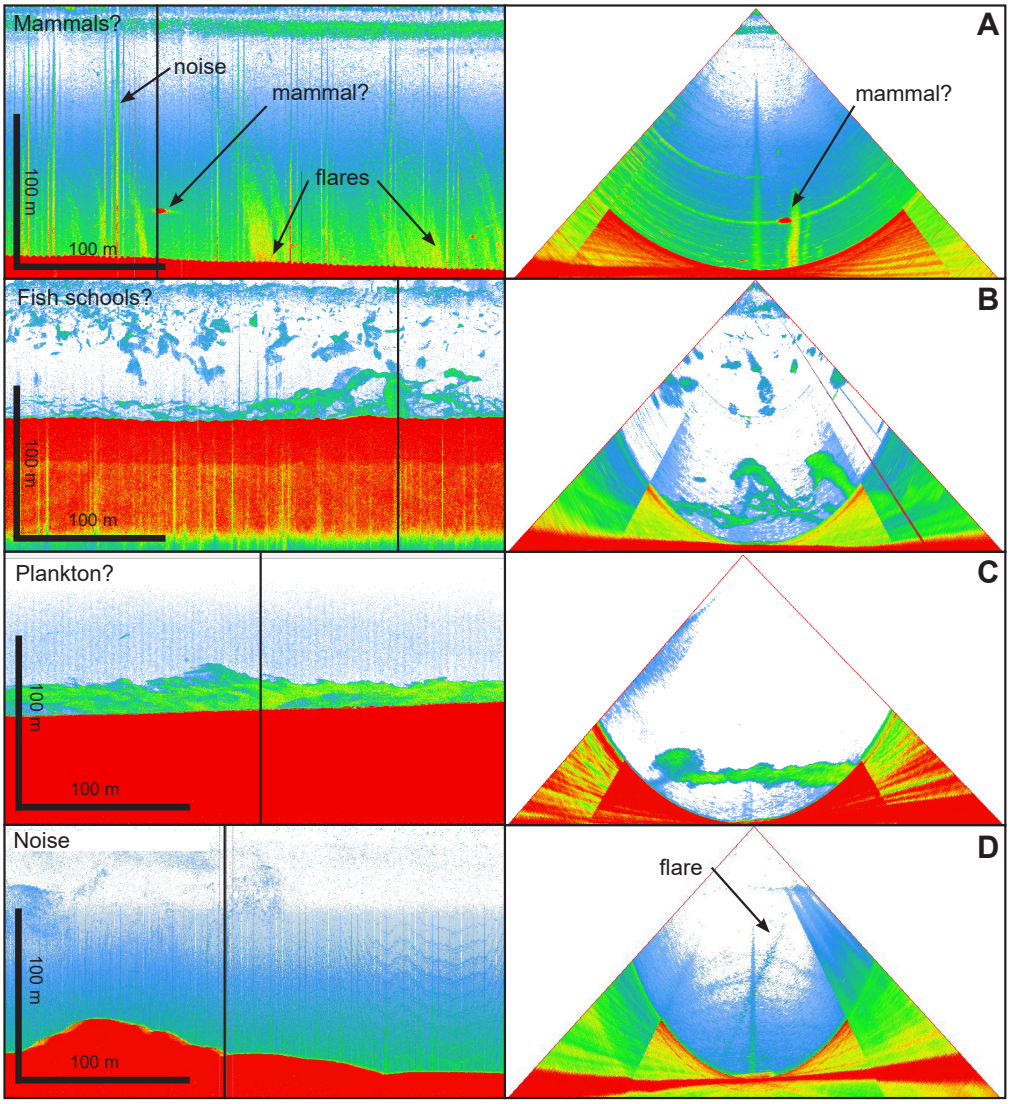

Figure 6. Examples of non-gas acoustic anomalies in water-column data. Left column displays along track, with black vertical line showing the location of across-track displays. Right column displays across track. (A) Possible mammals, together with gas flares and some vertical noise lines. (B) Possible fish schools. (C) Possible plankton clouds. D) Line with high noise level. Notice gas flare visible in the right column (arrow), but hardly visible in the left column.

Table 2. Codes used for assessment of magnitude.

Code	Description
1	Weak gas flare
2	Medium-strong gas flare
3	Strong gas flare
4	Very strong gas flare
5	Giant gas flare

Examples of gas flares with magnitudes from 1 to 5 are shown in Fig. 5. Generally, the recognition of gas flares is based on two criteria – the bubbles have higher backscatter strength than the ambient noise in the water-column data, and the objects with higher backscatter strength form characteristic patterns in the water column. Under ideal conditions, gas seeps may be observed as flare-shaped objects which start at the seabed and become narrower until they disappear at least 50–100 m above the seabed. If currents are sufficiently strong, the flares will be deflected. The identification of gas flares may be complicated due to several factors, such as high ambient (periodic or random) noise, fish shoals, high densities of plankton, strong and/or irregular currents, and sub-optimal intersection of the multibeam swath with the gas flare (i.e., covering only part of the flare). Examples of non-gas acoustic anomalies are shown in Fig. 6.

Results

Norwegian Sea shelf

The Norwegian Sea shelf (Fig. 7) forms the southernmost part of the studied area, where the main structural elements are the Trøndelag Platform, the Halten Terrace, deep Cretaceous basins, terraces and intra-cratonal elevations, a pre–Jurassic basin in the platform, Cretaceous highs, a marginal volcanic high, and several fault complexes (Blystad et al., 1995). Three hundred and seventy-nine gas flares were observed in this region. Most of the flares (293) occur in the Haltenbanken area, associated with the Halten Terrace. A cluster of 28 flares occur in the transition zone between the Grønøy High and the Vestfjorden Basin. Fifteen gas flares were observed in the Rås Basin, west of the Frøya High (Fig. 6). On the Måløy Slope, 39 flares were observed, forming a linear trend parallel to the southern end of the Møre–Trøndelag Fault Complex. One gas flare was observed between the Tampen Spur and the Ona High and is spatially associated with the Møre–Trøndelag Fault Complex. No gas flares have been observed on the Trøndelag Platform, in the deep Cretaceous basins east of the Halten Terrace, or in the transition between the Møre Volcanic High and the westernmost parts of the deep Cretaceous basin.

Many of the gas flares in the Halten Terrace area are spatially related to old exploration wells with 60% of the 57 gas flares located less than 20 m from an exploration well location (Table 3). Nearly 25% of these occur close to the Heidrun Field (Fig. 8).

Table 3. Distance between well location and gas flare, number of gas flares, and frequency.

Distance, m	No.	%
2–20	34	60
20–40	9	16
40–60	6	11
60–100	5	8
100–150	3	5

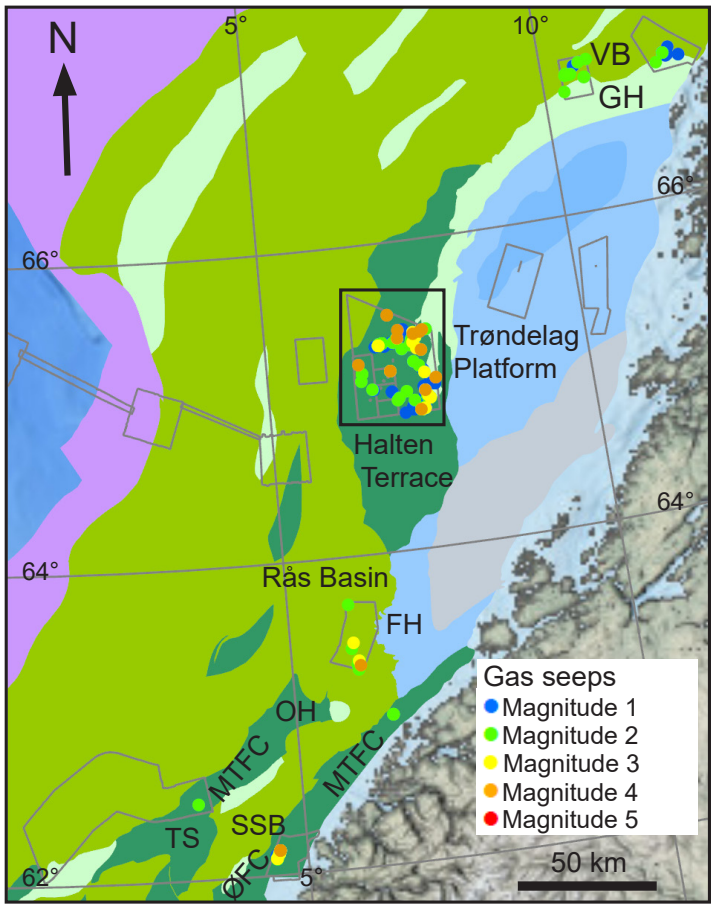

Figure 7. Distribution of gas flares on the Mid-Norwegian shelf in relation to major structural elements. Grey outlines show analysed areas. For legend, see figure 2. TS – Tampen Spur, SSB – Sløreboth Sub-basin, OH – Ona High, FH – Frøya High, ØFC – Øygarden Fault Complex, MTFC – Møre-Trøndelag Fault Complex, GH – Grønøy High, VB – Vestfjorden Basin.

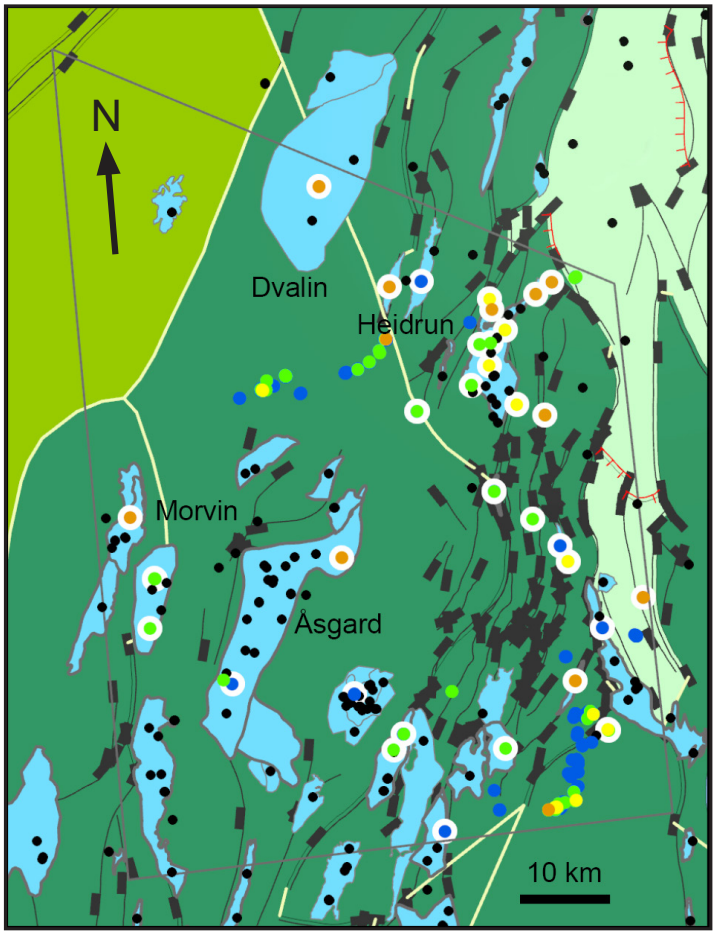

Figure 8. Gas flares in the Halten Terrace. White dots indicate the location of gas flares close to exploration well locations. Grey outline shows analysed area. Background map from NPD Factmaps (accessed 10.3.2022) showing wells (black dots), hydrocarbon fields (blue) and faults. For legend, see figures 2 and 7.

Southern Barents Sea and Lofoten area

The southern part of the Barents Sea and the Lofoten area (Fig. 9, between 68°45' and 73° N) includes the major structural elements such as the Finnmark Platform, the Harstad, Tromsø, Bjørnøya and Tiddly basins, the Loppa High, and the Troms–Finnmark, Ringvassøy–Loppa, and Bjørnøyrenna Fault complexes (Gabrielsen et al., 1990; Blystad et al., 1995). Most gas flares with confidence equal to or greater than 50% (144) are associated with the terrace between the Finnmark Platform and the Harstad Basin, located in the transition zone between the Troms–Finnmark and Ringvassøy–Loppa fault complexes. Twenty-one gas flares are found to the east of this area, on the Finnmark Platform (Fig. 9). Some gas flares (14) have also been mapped outside Vesterålen farther south, close to the Utrøst Ridge (not shown on map). No gas flares were observed within the Tiddlybanken Basin.

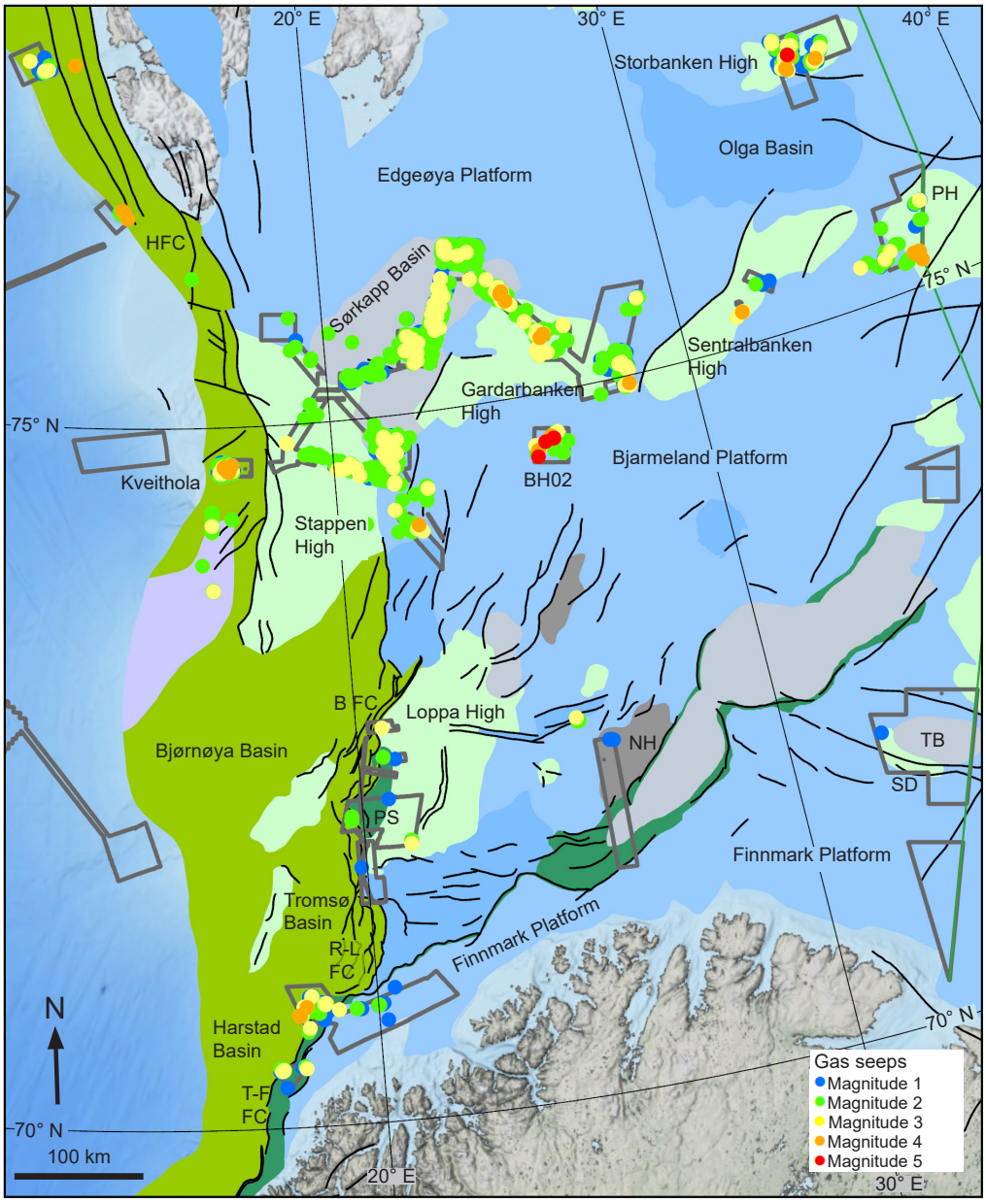

Figure 9. Structural elements in the southern and Central Barents Sea (from NPD Factmaps, accessed 10.3.2022), and gas flares. For legend, see figure 2. PS – Polheim Sub-platform, HFC – Hornsund Fault Complex, B FC – Bjørnøyrenna Fault Complex, R-L FC – Ringvassøy – Loppa Fault Complex, T-F FC – Troms-Finnmark Fault Complex, PH – Polarrev High, NH – Norsel High, TB – Tiddlybanken Basin. Dark grey outlines – analysed areas.

Another cluster of gas flares occurs in the transition zone between the westernmost part of the Loppa High and Bjørnøya Basin, where the Polheim Sub-platform and the Bjørnøyrenna Fault Complex (north) and Ringvassøy–Loppa Fault Complex are important structural elements (Fig. 9). A few possible gas flares have been found on the Norsel High.

Central Barents Sea

The central Barents Sea (between 73° and 77°30' N) includes major structural elements such as the Bjarmeland and Edgeøya platforms, the Bjørnøya (northern part), Sørkapp and Olga basins, the Stappen, Gardarbanken, Sentralbanken, Polarrev and Storbanken highs, and the Hornsund Fault Complex (Gabrielsen et al., 1990). A total of 3599 gas flares have been observed here (Fig. 9).

Most of the analysed areas are within the structural highs (Stappen High, Gardarbanken High, Sentralbanken High, Polarrev High and Storbanken High). The total analysed area within the highs is *c.* 9275 km^2, within which 696 gas flares have been observed, with an average density of 75 gas flares pr. 1000 km^2. The total area analysed within the basins (Sørkapp Basin, Fingerdjupet Sub-basin,) is *c.* 3000 km^2. The number of gas flares ranges from zero in the Fingerdjupet Sub-basin, to 968 gas flares found in the Sørkapp Basin (323 gas flares pr. 1000 km^2). The highest concentration of gas flares pr. 1000 km^2 was observed in Kveithola, *c.* 50 km WNW of Bjørnøya, where a deep Cretaceous basin is influenced by the Hornsund Fault Complex. Within a small area (360 km^2), as many as 525 gas flares have been reported, giving an average density of 1466 gas flares pr. 1000 km^2.

The Bjarmeland and Edgeøya platforms have been analysed only in limited areas. South of the Gardarbanken High on the Bjarmeland Platform in the area called BH02, 46 gas flares have been observed. 8 gas flares have been observed in the Edgeøya Platform, northeast of the Gardarbanken High.

Northern Barents Sea

The Northern Barents Sea (between 78° and 82°N) was only partly mapped by Gabrielsen et al. (1990), up to *c.* 80° N. In the western part, the deep Cretaceous basin influenced by the Hornsund Fault Complex dominates, while the Kong Karl Platform with anticlinal highs are found to the east (Fig. 10).

In the Vestnesa area, we have observed 26 gas flares at c. 1200 m water depth, extending up to 900 m from the seabed. At Sjubrebanken west of northern Spitsbergen, in the very northern end of the deep Cretaceous basin influenced by the Hornsund Fault Complex, we observed 162 gas flares, of which nearly 60% were classified as magnitude 4 or 5. The strongest gas flares align along a north–south trend, parallel to a major fault extending northwards from the area.

Around 651 gas flares have been observed north of Spitsbergen and Nordaustlandet, in Rijpfjorden, and on the shelf (northern part of Hinlopenrenna, on the shelf 75 km northeast of Hinlopenrenna, and north of Rijpfjorden), in Kvitøyrenna, and north of Kvitøya (Fig. 10). Most of the gas flares in Rijpfjorden (119) occur in an area where the bedrock is supposed to consist of 1.60–0.60 Ga old sandstones, conglomerates, claystone, some volcanic rocks and carbonates, according to Sigmond (2002). The gas flares on the shelf north of Rijpfjorden (176 gas flares) occur in areas with similar rocks plus gneisses of similar age. Many of the gas flares are classified as magnitude 5 flares and seem to reach the sea surface from water depths of between 225 and 150 m. The seafloor depth varies between 285 and 80 m with moderate topography, and a wide range of glacial structures such as iceberg plough marks and moraine ridges. No structures indicating the presence of crystalline bedrock have been observed.

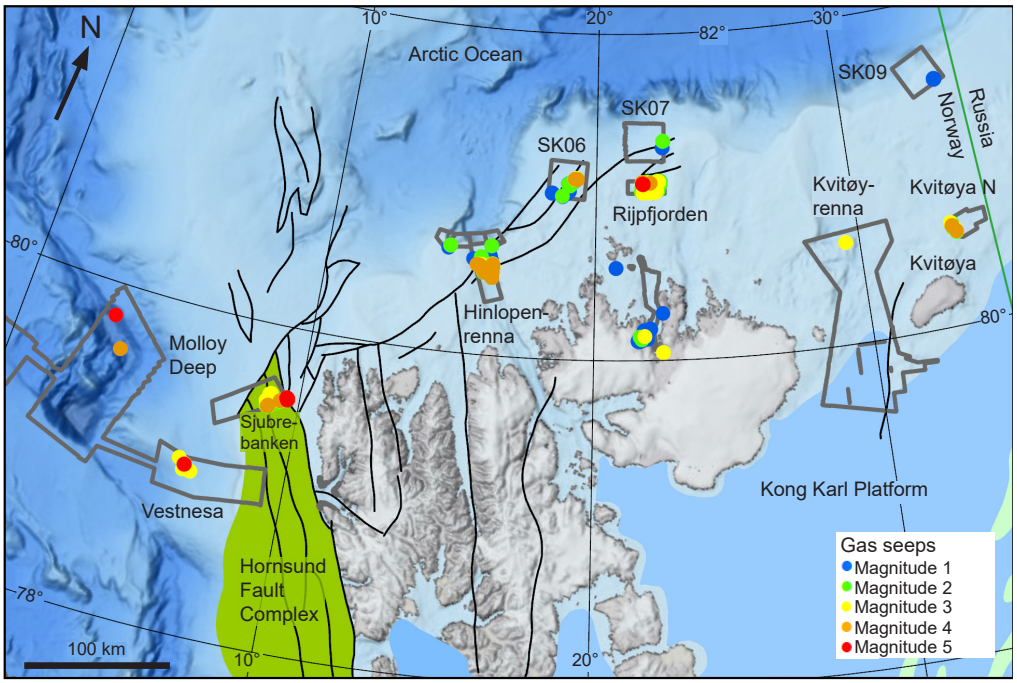

Figure 10. Structural elements in the northern Barents Sea and the southern part of the Arctic Ocean (from NPD Factmaps, accessed 10.3.2022), and gas flares. For legend, see figure 2. Dark grey outlines – analysed areas.

In contrast, the seafloor terrain in Kvitøyrenna is markedly different. The central and northwestern part of Kvitøyrenna is dominated by a rugged terrain, indicating that crystalline rocks sub-crop at the seafloor. A zoomed-in area (Fig. 11) in the northwestern part is dominated by rugged terrane, but with a *c.* 5 km-wide, E–W-trending belt of smooth topography in the southern part, and similarly smooth terrane in the northern part. The smooth belt in the southern part may represent a half-graben with sedimentary rocks, with an unconformity as the southern boundary, and a fault towards crystalline bedrock towards the north. Two gas flares occur in the northern part at the transition between rugged terrane and smooth terrane, possibly representing an unconformity (Fig. 11). However, it should be noted that the water column data have a high level of noise in many lines, which may have camouflaged other gas flares.

North of Kvitøya (Fig. 10), another 32 gas flares were observed in an area also supposedly consisting of 2.50–0.70 Ga metamorphic rocks (Sigmond, 2002). The seafloor has a low-relief morphology, and no rugged terrane, indicating that crystalline bedrock does not sub-crop at the seafloor.

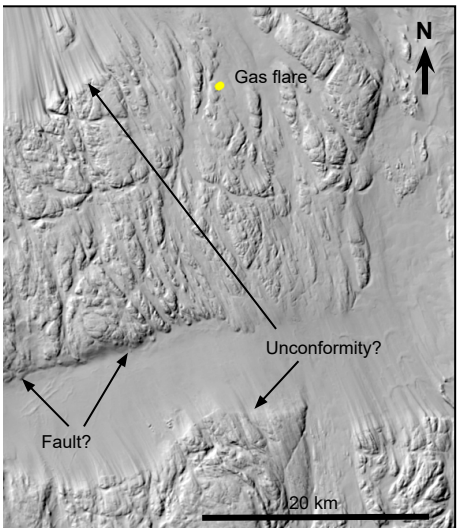

Figure 11. Shaded relief image from multibeam bathymetry showing proposed faults and unconformities and gas flares in the northern part of Kvitøyrenna.

Arctic Mid-Ocean Ridge and the Molloy Deep

Nearly 64 000 km^2 of multibeam water column data has been acquired and interpreted from the deep parts of the Norwegian Sea (Fig. 4A, B), but only two gas flares have been identified with a high degree of confidence (Molloy Deep) and one gas flare with 50% confidence in 2300 m water depth, approximately 100 km south of Jan Mayen (east of the area shown in Fig. 4).

The Molloy Deep (Fig. 12A) is ~3300 m deeper than the surrounding seabed at its deepest part and extends about 15 km x 15 km in dimension. The maximum water depth is 5569 m. The Molloy Ridge is located NNE of the Molloy Deep, reaching its shallowest part (~1500 m), with an elevation difference of approximately 4000 m, only 25 km from the Molloy Deep (Fig. 12A). The transform fault has three segments (Fig. 12A) with two blocks of highly fractured material filling the space in between and a further deformed zone west of it. The Molloy Deep occurs along the southern part of the transform fault and the region covering the southern part of the two blocks.

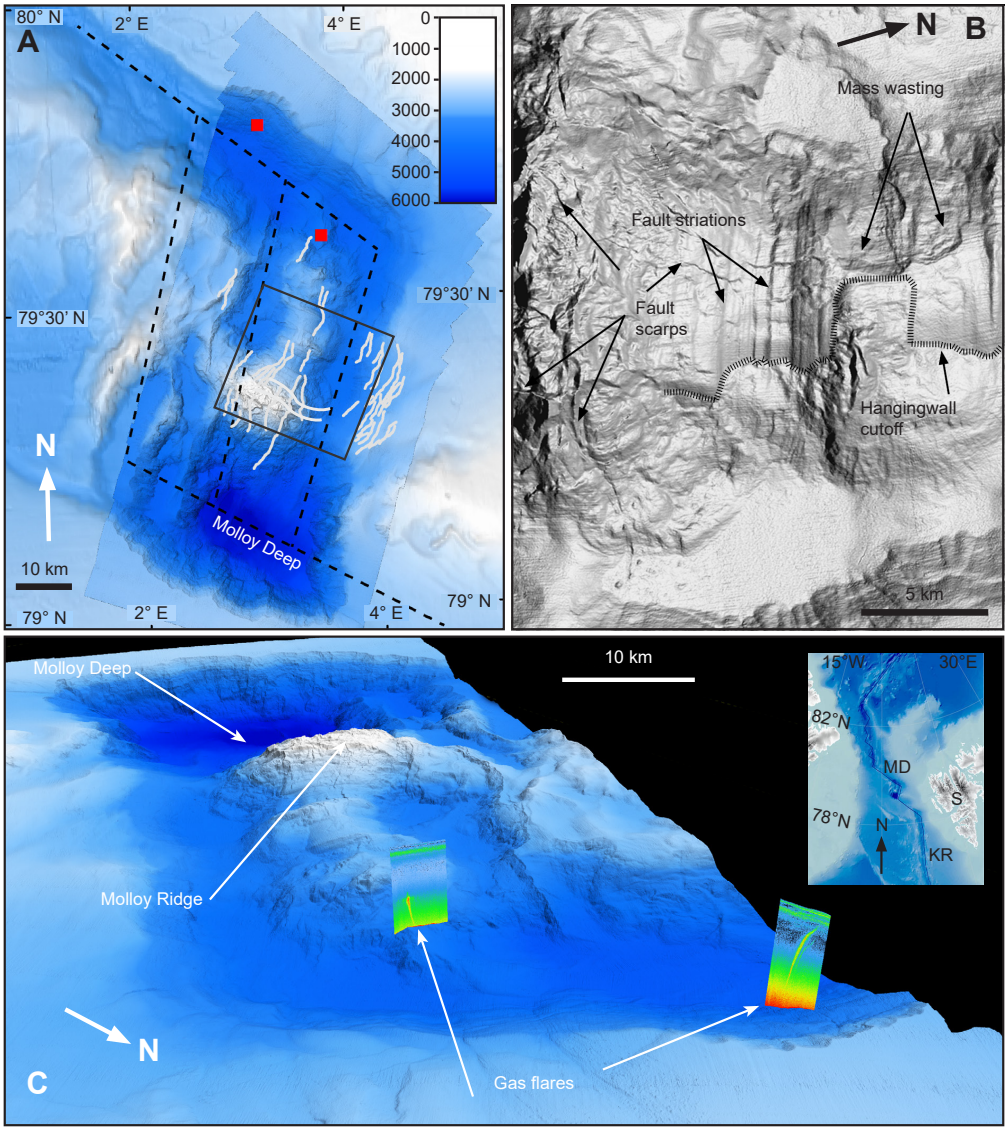

Figure 12. (A) Bathymetry of the Molloy Deep and nearby areas showing the complex structure of the ridge system (IBCAO). Gas flares are marked by red squares. The locations of faults observable on the bathymetry data are indicated by light grey lines and the three segments of the Mid Oceanic Ridge (MOR) fracture zone are indicated by black dashed lines. (B) Close-up of the Molloy core complex, showing the c. 1000 m high ridge with a hangingwall cutoff, fault striations, fault scarps and mass-wasting features. (C) 3D view of the Molloy Ridge and Molloy Deep, with side views of the gas flares. Inset map: MD – Molloy Deep; KR – Knipovich Ridge. S – Spitsbergen.

The central part of the Molloy Ridge appears to be a well-developed core complex, with an oceanic detachment fault forming a hangingwall cut off, a corrugated surface with fault striations, mass-wasting structures and steep brittle fault scarps (Fig. 12B). The observed structures are very similar to structures reported from oceanic core complexes at the Mid Atlantic Ridge (Escartin et al., 2017). The core is about 1000 m high, 12 km wide and slightly asymmetric with the steepest side towards WNW. Analysis of multibeam data indicates a very complex seafloor with many fractures running parallel to the fracture zone (Fig. 12A, B).

Two water-column acoustic anomalies were identified from this region (Fig. 12C). These gas flares are 1770 and 3355 m high and are located along the northernmost transfer fault. The water depths are 3524 m and 3924 m, respectively. The flares are located along the peripheries of the northern segment of the Molloy fracture zone. The northwestern flare (water depth 3924 m, height 3355 m) is located on the northern slope of the trough formed by the transfer fault. The average slope is 12° but varies between 5° and 30°. Several gullies occur on the slope, and the edge between the surrounding flat seafloor at *c*. 2575 m water depth and the slope is characterised by numerous slide scars which are up to 1000 m wide. Horizontal structures reminiscent of sedimentary layering occur (Fig. 12A). The southeastern flare (water depth 3524 m, height 1770 m) is located south of the northern transfer fault, in the northeastern extension of the Molloy Ridge. The seabed is chaotic, with slopes up to 45°. Slump structures and probably small gullies can be observed (Fig. 12A).

Discussion

Norwegian Sea shelf

The total number of gas flares in the surveyed area on the Norwegian Sea shelf is 379.

The highest density of gas flares occurs in the Haltenbanken area (Fig. 7), on the Halten Terrace, with 66 gas flares pr. 1000 km^2. This is in contrast to the rest of the area, where the average density is 9 gas flares pr. 1000 km^2.

The gas flares in the Haltenbanken area are spatially associated with faults (Fig. 8), and we suggest that the faults serve as conduits for fluids migrating from the reservoirs. Long-lived fluid migration associated with a vent complex on Haltenbanken, near the Heidrun field has been indicated by Garten et al. (2008). Petrological and isotope analyses of carbonate fragments from a well (6507/7–2) that penetrates limestone beds suggests that they represent seep carbonates from a methanogenic source, linked to early Tertiary reactivation of a fault defining a Triassic half graben. One of the gas flares observed in this study is located less than 5 m from this well position and may well be related to the vent complex. We have observed 57 gas flares closer than 150 m from exploration well positions. Thirty-four of these flares are located less than 20 m from the well positions. One possibility is that the well positions and gas flares are linked to sub-surface structures at reservoir depths. Another possibility is that the wells have triggered gas release from shallow gas accumulations, which are now seen as gas flares. Gas emissions from marine decommissioned hydrocarbon wells in the Central North Sea have been proposed to be linked to shallow gas accumulations and their distance to the wells (Böttner et al., 2020). In this study, drilling-induced fractures creating migration pathways are suggested to be the most important leaking mechanism. Alternative explanations involving natural leakages and well-integrity issues have been proposed by Wilpshaar et al. (2021), stating that the mechanism proposed by Böttner et al. (2020) is not properly supported by the results and leaves room for alternative interpretations. Gas flares associated with previously drilled exploration wells have been observed in the Barents Sea

(Mattingsdal et al., 2021). It should be noted that most of the gas flares observed in the Haltenbanken area have a magnitude of 1, 2 or 3, with only 12 gas flares with magnitude 4, and none with magnitude 5. The strongest gas flares (magnitude 4) are all associated spatially with the exploration wells.

In the same structural setting – terraces and intra-basinal elevations – 39 gas flares occur aligned with an NNE–SSW trend, parallel to the Møre–Trøndelag Fault Complex in the Slørebotn Sub-basin area (Fig. 7). As for the Halten Terrace, we suggest that faults serve as conduits for fluid flow.

Several gas flares (43) have been observed in the transition zones between basins (Vestfjorden Basin, Rås Basin) and nearby highs (Grønøy High, Frøya High). Faults along these margins are suggested to be conduits for fluid flow. No gas flares have been found on the Trøndelag Platform, probably owing to the stability in this area and lack of faults, or lack of source rocks.

Southern Barents Sea

The highest density of gas flares (105 gas flares pr. 1000 km^2) was observed on the terrace associated with the Troms–Finnmark Fault Complex between the Finnmark Platform and the Harstad Basin (Fig. 9). In the western parts of the Harstad Basin, seeps have been attributed to tilted Tertiary formations sub-cropping below glacial sediments, and high-amplitude seismic anomalies suggest the presence of gas pockets at the base of the glacial sediments and in the Tertiary deposits (Crémière et al., 2018).

In the eastern parts of the Harstad Basin, influenced by the Troms–Finnmark Fault Complex, gas seeps are suggested to originate from biodegraded thermogenic sources tentatively connected to the deeply faulted Mesozoic rocks. The difference in fluid sources is reflected by differences in carbon isotope data from authigenic carbonate crusts (Crémière et al., 2018).

On the Finnmark Platform east of the terrace associated with the Troms–Finnmark Fault Complex, 21 gas flares were observed. They are located along an ENE–WSW trend, sub-parallel to the Troms–Finnmark Fault Complex, and we suggest that these gas flares are fault-related. The platform areas in the eastern parts of the southern Barents Sea (Fig. 9), along the border towards Russia, have no gas flares. This could be due to stability in this area and lack of faults, or lack of source rocks. One gas flare was observed close to the boundary between the Finnmark Platform and the Signalhorn Dome, possibly associated with faults.

Several gas flares occur in the Polheim Sub-Platform and Loppa High, bounded westwards by the Ringvassøy–Loppa Fault Complex in the south, and the Bjørnøyarenna Fault Complex in the north. The gas flares are spatially associated with the faults in the fault complexes, and Chand et al. (2012*a*) indicated that the faults serve as conduits for fluid flow. Unloading due to erosion and deglaciation resulted in the opening of pre-existing faults and the creation of new ones, facilitating fluid flow to the seabed.

Central Barents Sea

The gas flares in the central Barents Sea (Figs. 9 & 13), can roughly be grouped into the following areas of occurrence:

- Structural highs, where Middle to Late Triassic reservoir rocks subcrop at the seabed or beneath the glacial sediments (Stappen High, Gardarbanken High, Sentralbanken High, Polarrev High and Storbanken High).

- Deep Cretaceous basins affected by the Hornsund Fault Complex and the Bjørnøyrenna/Ringvassøy–Loppa/Troms–Finnmark fault complexes (in the western parts).
- The pre–Jurassic Sørkapp Basin, covered by Late Jurassic to Cretaceous sedimentary rocks.
- Transition zone from Middle to Late Triassic to Cretaceous sedimentary rocks within the Bjarmeland Platform, south of the Gardarbanken High.

The total area of water-column data analysed within the structural highs is *c.* 9275 km^2, and 696 gas flares have been observed, giving an average density of 75 gas flares pr. 1000 km^2. The highs expose Middle to Late Triassic reservoir rocks at the seabed beneath glacial sediments of varying thickness (Fig. 13) and are evidently an important setting for bringing fluids up to the seabed and into the water column. Faulting will be associated with the highs, and we suggest that this will be an important secondary mechanism for fluid flow. Several anticlinal structures on the Sentralbanken High with eroded tops exposing reservoirs of the Middle Triassic Kobbe Formation provide important 'windows' for extensive fluid discharge (Serov et al., 2023). Faults on the flanks of the structural highs were found to correlate with seepage, while faults in the apex of the Sentralbanken High did not show any consistent correlation between faulting and seeping (Serov et al., 2023).

The highest number of gas flares per area is found in Kveithola, where as many as 525 gas flares occur within an area of only 360 km^2, giving an average density of 1466 gas flares per 1000 km^2. The structural setting is a deep Cretaceous basin, affected by the Hornsund Fault Complex. Mau et al. (2017) reported over a thousand gas flares from Bjørnøya to Kongsfjordrenna, with most flares in the vicinity of the Hornsund Fault Complex. This included a few gas flares in Kveithola. Extensive seafloor gas seepage associated with the Hornsund Fault Complex was found in Storfjordrenna *c.* 150 kilometres north of Kveithola (Waage et al., 2019), We suggest that faults within the Hornsund Fault Complex serve as conduits for fluid flow from sub–Cretaceous source rocks.

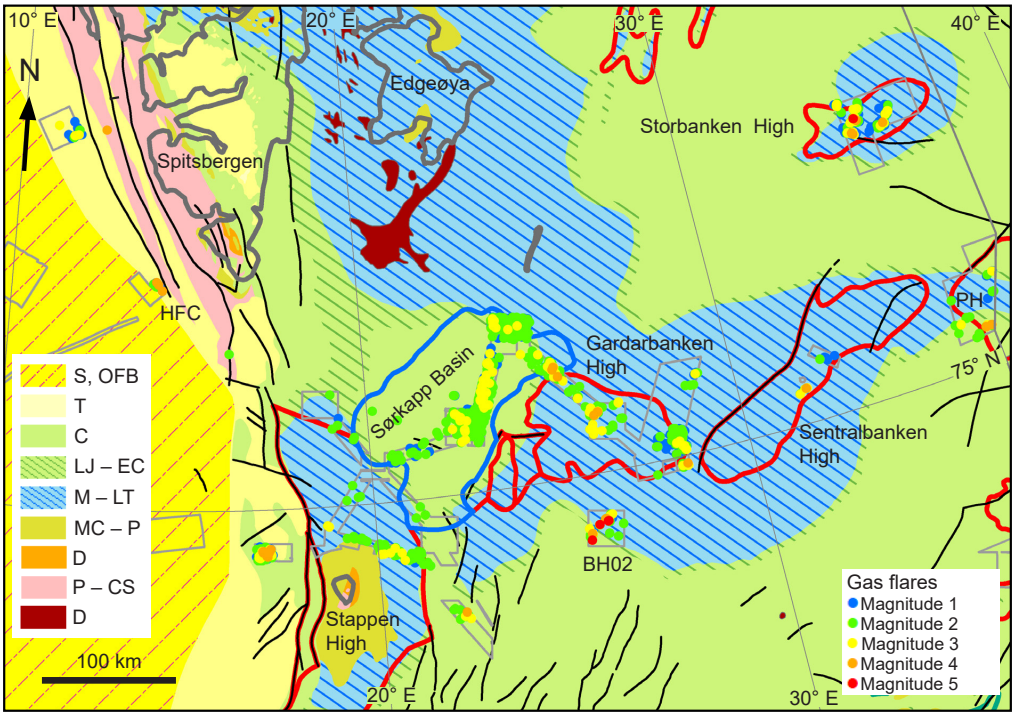

Figure 13. Outcropping bedrock (simplified from Sigmond (1992), gas flares, selected structural elements and faults in the central Barents Sea (from NPD 2022). HFC – Hornsund Fault Complex. PH – Polarrev High. S, OFB – Sedimentary rocks with underlying Tertiary ocean floor basalts; T – Tertiary; C – Cretaceous; LJ – EC – Late Lurasssic to Early Cretaceous; M – LT – Mainly Mid to Late Triassic; MC – P – Mid Carboniferous to Permian; D – Devonian; P – CS – Proterozoic to Cambro-Silurian metamorphic rocks; D – Diabase, locally basalt, Triassic – Early Cretaceous.

The total area analysed within the basins (Sørkapp Basin, Fingerdjupet Sub-basin, Olga Basin) is *c.* 5060 km^2. The number of gas flares range from zero in the Olga Basin and Fingerdjupet Sub-basin, which are shallow Cretaceous basins in the Platform, to 968 gas flares in the Sørkapp Basin (323 gas flares per 1000 km^2), which is a pre–Jurassic basin in the platform. The Sørkapp Basin has an unexpected high number of gas flares. The reasons for that are not fully understood, but seismic interpretation from the Sørkapp Basin indicates a thick Mesozoic succession (Anell et al., 2014; Lundschien et al., 2014), including a N–S-trending Lower to Middle Triassic depocentre, with thick sedimentary sequences lining up with the excellent oil and gas source rock areas of Svalbard and the Loppa High. Using a time/depth relation of 1.45 for the Loppa High from seabed down to base Permian Wells 7120/2–1 and 7222/1–1, a maximum present burial depth of up to 1000–1800 ms TWT in the Sørkapp Basin (based on Anell et al., 2014), corresponds to 1450–2600 m. Based on maps from Henriksen et al. (2011) and Lasabuda et al. (2021), this area has been uplifted more than 2000 m during the Late Cenozoic, indicating up to 3450 to 4600 m maximum burial; with a temperature gradient of 35°C/km the corresponding temperatures will have been 120°C to 160°C. This means that Lower to Middle Triassic source rocks of the Sørkapp Basin here would have reached well into the oil and gas window. Based on this it seems a plausible hypothesis that the observed gas flares in the Sørkapp Basin could represent gas, and possibly oil, from a Lower to Middle Triassic hydrocarbon system that has been leaking since maximum burial, which may have accelerated during the Pleistocene rebound.

The gas flares observed to the south of the Gardarbanken High, in the sub-area called BH02 (Figs. 9 & 13), occur within the Bjarmeland Platform. Here, Middle to Late Triassic source rocks and carrier beds overlain by Cretaceous deposits dipping from north to south are subcropping under the Pleistocene sediment cover or are subcropping directly at the seabed. We interpret this to be another example of ongoing migration of fluids from subcropping Triassic reservoir rocks, carrying fluids from a deeper Triassic source rock.

Northern Barents Sea

The Vestnesa gas seeps (e.g., Bünz et al., 2012, Panieri et al., 2017) have been interpreted to result from hydrate-modulated methane seepage. Maturation of Miocene rocks is likely to be the origin of the gas in this area and seepage could have started in the Early Pleistocene, more than 2 Ma ago (Knies et al., 2018); abiotic methane has also been suggested (Johnson et al., 2015). However, the suggestion for abiotic methane was not supported by Panieri et al. (2017) who reported that the gas from the Vestnesa system has both microbial and thermogenic sources, with a predominantly mixed gas signature of methane in both of the sampled pockmarks (Lomvi and Lunde). 162 gas flares are found north of Sjubrebanken (Fig. 10), in the northern part of the Deep Cretaceous Basin affected by the Hornsund Fault Complex. Most of the gas flares (65%) align along a north–south trend, parallel to a major fault extending northwards from the area. These gas flares are also the strongest, with most of the gas flares having magnitude 4 or 5. It seems clear that the faults within the Hornsund Fault Complex serve as conduits for fluid flow from gas-producing source rocks. There are also seismic studies indicating the presence of free gas in the crestal parts of buried ridges north of Sjubrebanken (Mattingsdal et al., 2014), and several other seismic studies on the Yermak Plateau north of Sjubrebanken have indicated the presence of free gas (Geissler & Jokat, 2004; Jokat et al., 2008).

The bedrock geology on the shelf north of Spitsbergen and Nordaustlandet has not been mapped in detail, and this may explain why 75% of the 651 gas flares observed in this area are located within supposedly 2.5–0.70 Ga metamorphic rocks. The smooth seabed morphology in the Hinlopen area, and on the shelf north of Rijpfjorden indicates that the substrate is not composed of metamorphic rocks. The seabed morphology in the northern part of Kvitøyrenna (Fig. 11) indicates that a system

of half-grabens with unconformities and faults underlie this area. The single gas flare observed in Kvitøyrenna is located at the transition between rugged and smooth terrane and may represent seepage along basal beds above the proposed unconformity.

The gas flares on the shelf (Hinlopenrenna, SK06, SK07, SK09) tend to align along ENE–WSW trends parallel to the faults (Fig. 10), and we suggest that the faults have served as conduits for migrating fluids.

Most of the acoustic anomalies in the Rijpfjorden area resemble what we commonly interpret as gas flares, but their character is more variable, and generally we have assigned a low confidence (50%) for most of the anomalies, meaning that we consider an equal probability for the acoustic anomalies to be gas flares or something else (Fig. 14). In many cases, some biological phenomena (plankton, fish, mammals) will be the cause for such acoustic anomalies. Particularly in fjord environments, we need to consider groundwater discharge as well, noting that groundwater discharges also can occur on the continental shelf and slope (Hong et al., 2019). According to the bedrock map (Sigmond, 2002), the geology of this area comprises sandstone, conglomerate and claystone, as well as some volcanic and carbonate rocks, with ages of 1.60–0.6 Ga. It is considered unlikely that such rocks could produce gas giving rise to these acoustic anomalies. Down-faulted sedimentary rocks of Paleozoic to Mesozoic age capable of producing gas could be an alternative explanation, but inspection of aerial imagery (ESRI ArcGIS Online and data partners, including imagery from agencies supplied via the Content Sharing Program), looking for indications of fault structures, leaves this as an unlikely option. For the time being, the source and mechanisms for the acoustic anomalies in Rijpfjorden cannot be explained.

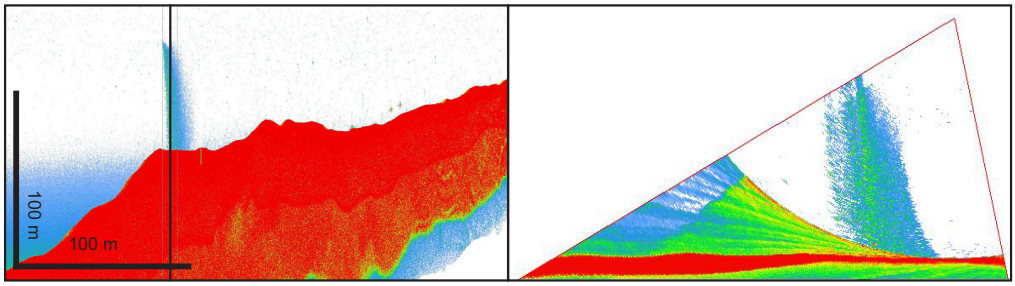

Figure 14. Gas flare of uncertain origin in Rijpfjorden. Left column: gas flare along the track lines. Black line shows position of the section in the right column. Right column: gas flare in the beam fan (perpendicular to track line).

Molloy Deep

Two large gas flares, 1770 m and 3550 m high, have been observed in the Molloy area (Fig. 12A, C). The presence of the gas flares and their heights in the water column indicate that the seep locations are in the gas hydrate stability zone, and that there are hydrate coatings on the bubble walls, reducing the rate of dissolution of methane in seawater (McGinnis et al., 2006).

The northwestern gas flare in the Molloy area (Fig. 12C) originates on the northern slope of the northernmost transfer fault, where horizontal structures, gullies and slide scars may indicate that sedimentary rocks subcrop in this area, and it is therefore suggested that the gas seep shown by the gas flare originates from sedimentary rocks of possible Miocene age.

The southeastern flare originates from a tectonically active area where the seabed is chaotic with mass wasting features and fault scarps and slopes up to 45°. We propose, based on the surface structures, that the rocks subcropping in this area are sedimentary rocks which have been uplifted and faulted by the northern extension of the Molloy Ridge core complex. During a ROV dive with ÆGIR 6000 in June 2022, condensate oil seeping from the seabed at the base of the southeastern flare was sampled (R.B. Pedersen, pers.comm, 2023).

A thermogenic source for this gas seep similar to the northern flare is held as the most probable; however, an abiotic origin could be possible since the flare occurs along the northern part of the core complex within the active spreading Molloy Ridge. Slow spreading ridges, and in this case along the transform fault, are suggested to have elevated methane generation and release because of serpentinisation (Charlou et al., 2010). Serpentinisation due to circulation of seawater deep into the mantle is inferred since mantle rocks are shallow there (<5 km) and deep faults do exist (Kandilarov et al., 2008).

The Molloy Ridge is suggested to be a slow to ultra-slow spreading ridge and therefore serpentinisation may have occurred along detachment faults over a period of 1–4 million years (Tucholke et al., 1998). The rocks at the base of the flares from Molloy also fall within this age range based on spreading rate since the separation of Greenland from Svalbard. A similar process is suggested to be the source of methane from the nearby Knipovich Ridge, where gas hydrate related anomalies are observed on seismic data (Rajan et al., 2012; Johnson et al., 2015). The region needs to be further investigated with deep seismic and ROV to confirm the processes behind the formation of these flares.

Conclusions

Water-column data acquired with multibeam echosounders in the MAREANO program across 136 000 km^2 of the Norwegian EEZ have been interpreted and more than 5000 gas flares have been identified. Geological structures impose a strong control on the distribution, number and intensity of gas flares, and the number of gas flares pr. 1000 km^2 ranges from 0 to over 1000. Most of the gas flares are considered to originate from either biogenic, thermogenic or mixed origin sources. Biodegradation of thermogenic gas has been observed.

Faults serving as conduits for fluid flow seem to be the most important source for fluid flow in areas such as the Halten Terrace on Haltenbanken, the terrace associated with the Troms–Finnmark Fault Complex between the Harstad Basin and the Finnmark Platform, and in the western part of the Loppa High. Structural highs exposing Triassic to Jurassic carrier rocks at the seabed (including those buried under glacial sediments) that are associated with faults along the flanks are an important mechanism in the central Barents Sea, including the Stappen, Gardarbanken, Sentralbanken, Storbanken and Polarrev highs.

Tilted reservoir rocks subcropping at the seabed are an important source for fluid flow in some places, such as the western part of the Harstad Basin, and south of the Gardarbanken High, where dipping Middle to Late Triassic source rocks and carrier beds are subcropping beneath the Pleistocene sediment cover or lying directly at the seabed.

Many of the gas flares observed in the Haltenbanken area are spatially associated with abandoned exploration wells, but the causes are uncertain. The gas flares in the Molloy Deep are suggested to originate from sedimentary rocks of possible Miocene age, but an abiotic origin cannot be ruled out for the gas flare at the northern extension of the Molloy Ridge core complex.

The acoustic anomalies in the Rijpfjorden area on Nordaustlandet, located above subcropping Precambrian sedimentary rocks, have an unknown origin, and unknown mechanism for fluid flow.

Acknowledgements. MAREANO, Aker BP and the Norwegian Defence Research Establishment are gratefully acknowledged for permission to publish these data. The reviewers are thanked for their very constructive comments. Detailed bathymetry was supplied by MAREANO/Norwegian Mapping Authority.

References

Anell, I., Braathen, A. & Olaussen, S. 2014: Regional constraints of the Sørkapp Basin: A Carboniferous relic or a Cretaceous depression? *Marine and Petroleum Geology 54*, 123–138, https://doi.org/10.1016/j.marpetgeo.2014.02.023

Aiuppa, A., Hall-Spencer, J.M., Milazzo, M., Turco, G., Caliro, S. & Di Napoli, R. 2021: Volcanic CO2 seep geochemistry and use in understanding ocean acidification. *Biogeochemistry 152*, 93–115. https://doi.org/10.1007/s10533–020–00737–9

Aloisi, G., Bouloubassi, I., Heijs, S.K., Pancost, R.D., Pierre, C., Sinninghe Damste, J.S., Gottscal, J.C., Forney, L.J. & Rouchy, J.-M., 2002 : CH4-consuming microorganisms and the formation of carbonate crusts at cold seeps. *Earth Planet Science Letters 203*, 195–203. https://doi.org/10.1016/S0012-821X(02)00878-6

Andreassen, K., Laberg, J. S. & Vorren, T. O. 2008: Seismic seafloor geomorphology of the SW Barents Sea and its glaci-dynamic implications. *Geomorphology 97*, 157–177. https://doi.org/10.1016/j.geomorph.2007.02.050

Andreassen, K., Hubbard, A., Winsborrow, M., Patton, H., Vadakkepuliyambatta, S., Plaza-Faverola, A., Gudlaugsson, E., Serov, P., Deryabin, A., Mattingsdal, R., Mienert, J. & Bünz, S. 2017: Massive blow-out craters formed by hydrate-controlled methane expulsion from the Arctic seafloor. *Science 356*, 948–953. https://doi.org/10.1126/science.aal4500

Betlem, P., Roy, S., Birchall, T., Hodson, A., Noormets, R., Römer, M., Skogseth, R. & Senger, K. 2021: Modelling of the gas hydrate potential in Svalbard's fjords. *Journal of Natural Gas Science and Engineering, 94,* 104127, https://doi.org/10.1016/j.jngse.2021.104127

Blystad, P., Brekke, H, Færseth, R.B., Larsen, B.T, Skogseid, J. & Tørudbakken,B. 1995: Structural elements of the Norwegian continental shelf. Part II: The Norwegian Sea Region. *NPD Bulletin No 8*.

Brunstad, H. & Rønnevik, H.C. 2022: Loppa High Composite Tectono-Sedimentary Element, Barents Sea. *Geological Society, London, Memoirs 57*. https://doi.org/10.1144/M57-2020-3

Bünz, S., Polyanov, S., Vadakkepuliyambatta, S., Consolaro, C. & Mienert, J. 2012:
Active gas venting through hydrate-bearing sediments on the Vestnesa Ridge, offshore W–Svalbard. *Marine Geology 334,* 189–197. https://doi.org/10.1016/j.margeo.2012.09.012

Böttner, C., Haeckel, M., Schmidt, M., Berndt, C., Vielstädte, L., Kutsch, J.A., Karstens, J. & Weiß, T. 2020: Greenhouse gas emissions from marine decommissioned hydrocarbon wells: leakage detection, monitoring and mitigation strategies. *International Journal of Greenhouse Gas Control 100*, 103119, https://doi.org/10.1016/j.ijggc.2020.103119

Campbell, K. A. 2006: Hydrocarbon seep and hydrothermal vent paleoenvironments and palaeontology: Past developments and future research directions. *Palaeogeography, Palaeoclimatology, Palaeoecology 232,* 362–407. https://doi.org/10.1016/j.palaeo.2005.06.018

Chand, S. & Thorsnes, T. 2020: Processing and interpretation of water column data from the Polarrev High, Barents Sea. *NGU Report 2020.025,* 116 pp.

Chand, S., Mienert, J., Andreassen, K., Knies, J., Plassen, L. & Fotland, B., 2008: Gas hydrate stability zone modelling in areas of salt tectonics and pockmarks of the Barents Sea suggest an active hydrocarbon venting system. *Marine and Petroleum Geology 25*, 625–636. https://doi.org/10.1016/j.marpetgeo.2007.10.006

Chand, S., Thorsnes, T., Rise, L., Brunstad, H., Stoddart, D., Bøe, R., Lågstad, P. & Svolsbru, T. 2012*a*: Multiple episodes of fluid flow in the SW Barents Sea (Loppa High) evidenced by gas flares, pockmarks and gas hydrate. *Earth and Planetary Science Letters 333*, 305–314. https://doi.org/10.1016/j.epsl.2012.03.021

Chand, S., Thorsnes, T., Rise, L. & Bøe, R. 2012b: Pockmarks, gas flares, tectonic features and processes leading to their formation, southwestern Barents Sea. *NGU Report 2012.017*, 28 pp.

Chand, S., Thorsnes, T., Rise, L., Brunstad, H. & Stoddart, D. 2016: Pockmarks in the SW Barents Sea and their links with iceberg ploughmarks. *In* Dowdeswell, J.A., Canals, M., Jakobsson, M., Todd, B. J., Dowdeswell, E. K. & Hogan, K. A. (eds.). *Atlas of Submarine Glacial Landforms: Modern, Quaternary and Ancient*. Geological Society, London, Memoirs 46, 295–296, http://doi.org/10.1144/M46.23

Chand, S., Crémière, A., Lepland, A., Thorsnes, T., Brunstad, H. & Stoddart, D. 2017: Long-term fluid expulsion revealed by carbonate crusts and pockmarks connected to subsurface gas anomalies and palaeo-channels in the central North Sea. *Geo-Marine Letters 37*, 215–227. https://doi.org/10.1007/s00367-016-0487-x

Charlou, J.L., Donval, J.P., Konn, C., Ondreas, H., Fouquet, Y., Jean-Baptiste, P. & Fourre, E. 2010: High production and fluxes of H_2 and CH_4 and evidence of abiotic hydrocarbon synthesis by serpentinization in ultramafic-hosted hydrothermal systems on the Mid-Atlantic Ridge. *In* Rona, P. et al. (eds.) *Diversity of Hydrothermal Systems on Slow Spreading Ocean Ridges*. Geophysical Monograph Series, vol. 188, pp. 265–296, AGU, Washington, D. C. https://doi.org/10.1029/2008GM000752

Crémière, A., Chand, S., Sahy, D., Condon, D., Noble, S.R., Martma, T., Thorsnes, T., Sauer, S. & Brunstad, H. 2016: Timescales of methane seepage on the Norwegian margin following collapse of the Scandinavian Ice Sheet. *Nature Communications 7,* 11509. https://doi.org/10.1038/ncomms11509

Crémière, A., Chand, S., Sahy, D., Thorsnes, T., Martma, T., Noble, S.R., Pedersen, J.H., Brunstad, H. & Lepland, A. 2018: Structural controls on seepage of thermogenic and microbial methane since the last glacial maximum in the Harstad Basin, southwest Barents Sea. *Marine and Petroleum Geology 98*, 569–581. https://doi.org/10.1016/j.marpetgeo.2018.07.010

Czuba, W., Ritzmann, O., Nishimura, Y., Grad, M., Mjelde, R., Guterch, A. & Jokat, W. 2005: Crustal structure of northern Spitsbergen along the deep seismic transect between the Molloy Deep and Nordaustlandet, *Geophysical Journal International 161*, 347–364. https://doi.org/10.1111/j.1365-246X.2005.02593.x

Dalland, A., Worsley, D. & Ofstad, K. 1988: A Lithostratigraphic Scheme for the Mesozoic and Cenozoic and Succession Offshore Mid- and Northern Norway, Oljedirektoratet, *NPD Bulletin No. 4*, 87 pp.

Damm, E., Mackensen, A., Budéus, G., Faber, E. & Hanfland, C. 2005: Pathways of methane in seawater: Plume spreading in an Arctic shelf environment (SW–Spitsbergen). *Continental Shelf Research 25*, 1453–1472. https://doi.org/10.1016/j.csr.2005.03.003

Eidvin, T., Jansen, E. & Riis, F. 1993: Chronology of Tertiary fan deposits off the western Barents Sea: Implications for the uplift and erosion history of the Barents shelf. *Marine Geology 112*, 109–131. https://doi.org/10.1016/0025-3227(93)90164-Q

Eiken, O. & Hinz, K., 1993: Contourites in the Fram Strait. *Sedimentary Geology 82*, 15–32. https://doi.org/10.1016/0037-0738(93)90110-Q

Engen, Ø., Eldholm, O. & Bungum, H. 2003: The Arctic plate boundary. *Journal of Geophysical Research 108*, 2075. https://doi.org/10.1029/2002JB001809

Escartin, J., Mevel, C., Petersen, S., Bonnemains, D., Cannat, M., Andeani, M., Augustin, N., Bezos, A., Chavagnac, V., Choi, Y., Godard, M., Haaga, K., Hamelin, C., Ildefonsa, B., Jamieson, J., John, B., Leleu, T., MacLeod, C.J., Massot-Campos, M., Nomikou, P., Olive, J.A., Paquet, M., Rommevaux, C., Rothenbeck, M., Steinfuhrer, Tominaga, M., Triebe, L., Campos, R., Gracias, N. & Garcia, R. 2017: Tectonic structure, evolution, and the nature of oceanic complexes and their detachment zones (13° 20/N and 13° 30/N, Mid Atlantic Ridge). *Geochemistry, Geophysics, Geosystems 18*, 1451-1582. https://doi.org/10.1002/2016GC006775.

Faleide, J.I., Tsikalas, F., Breivik, A., Mjelde, R., Ritzmann, O., Engen, Ø., Wilson, J. & Eldholm, O. 2008: Structure and evolution of the continental margin off Norway and the Barents Sea. *Episodes 31*, 82–91. https://doi.org/10.18814/epiiugs/2008/v31i1/012

Gabrielsen, R.H, Færseth, R.B, Jensen L.N., Kalheim J.E. & Riis, F. 1990: Structural elements of the Norwegian continental shelf part I: the Barents Sea region. *NPD Bulletin No. 6*.

Gabrielsen, R.H., Grunnaleite, I., & Rasmussen, E. 1997: Cretaceous and Tertiary inversion in the Bjørnøyrenna Fault Complex, south–western Barents Sea. *Marine and Petroleum Geology 14*, 165–178. https://doi.org/10.1016/S0264-8172(96)00064-5

Gac, S., Minakov, A., Shephard, G. E., Faleide, J. I., & Planke, S. 2020: Deformation analysis in the Barents Sea in relation to Paleogene transpression along the Greenland-Eurasia plate boundary. *Tectonics 39.* https://doi.org/10.1029/2020TC006172

Gaina, C. 2014: Plate reconstructions and regional kinematics. *In* Hopper J.R., Funck T., Stoker M., Árting U., Péron-Pinvidic G., Doornenbal J.C. & Gaina C. (eds.) *Tectonostratigraphic Atlas of the North–East Atlantic Region*. Geological Survey of Denmark and Greenland (GEUS), Copenhagen, Denmark, 53–66.

Garten, P., Houbiers, M., Planke, S. & Svensen, H. 2008: Vent complex at Heidrun. *Seg Technical Program Expanded Abstracts 27*. https://doi.org/10.1190/1.3063767

Geissler, W. & Jokat, W. 2004: A geophysical study of the northern Svalbard continental margin. *Geophysical Journal International 158*, 50–66. https://doi.org/10.1111/j.1365-246X.2004.02315.x

Gernigon, L., Brönner, M., Roberts, D., Olesen, O., Nasuti, A., & Yamasaki, T. 2014: Crustal and basin evolution of the southwestern Barents Sea: From Caledonian orogeny to continental breakup. *Tectonics 33*. https://doi.org/10.1002/2013TC003439

Greinert, J., Bohrmann, G. & Suess, E. 2001: Gas Hydrate-Associated Carbonates and Methane-Venting at Hydrate Ridge: Classification, Distribution and Origin of Authigenic Lithologies. *In* Paull, C.K and Dillon, P.W. (eds.): *Natural Gas Hydrates: Occurrence, Distribution and Detection. Geophysical Monograph 124*, 99–113. https://doi.org/10.1029/GM124p0099

Greinert, J., Artemov, Y., Egorov, V., De Batist, M. & McGinnis, D. 2006: 1300-m-high rising bubbles from mud volcanoes at 2080 m in the Black Sea: Hydroacoustic characteristics and temporal variability. *Earth and Planetary Science Letters 244*, 1–15. https://doi.org/10.1016/j.epsl.2006.02.011

Grogan, P., Østvedt-Ghazi, A.-M., Larssen, G. B., Fotland, B., Nyberg, K., Dahlgren, S. & Eidvin, T. 1999: Structural elements and petroleum geology of the Norwegian sector of the northern Barents Sea. *In* Fleet, A. J. & Boldy, S. A. R. (eds.) *Petroleum Geology of Northwest Europe: Proceedings of the 5th Conference*, 247–259. https://doi.org/10.1144/0050247

Gudlaugsson, S.T., Faleide, J.I., Johansen, S.E. & Breivik, A.J. 1998: Late Palaeozoic structural development of the South–western Barents Sea. Marine and Petroleum Geology 15, 73–102. https://doi.org/10.1016/S0264-8172(97)00048-2

Henriksen, E., Bjørnseth, H. M., Hals, T. K., Heide, T., Kiryukhina, T., Kløvjan, O. S., Larssen, G. B., Ryseth, A. E., Rønning, K., Sollid, K. & Stoupakova, A. 2011: Uplift and erosion of the greater Barents Sea: impact on prospectivity and petroleum systems. *In* Spencer, A. M., Embry, A. F., Gautier, D. L., Stoupakova, A. V. & Sørensen, K. (eds.) *Arctic Petroleum Geology*. Geological Society, London, Memoirs, 35, 271–281. The Geological Society of London 2011. https://doi.org/10.1144/M35.17

Hong, W.-L., Lepland, A., Himmler, T., Kim, J.-H., Chand, S., Sahy, D., Salomon, E. A., Rae, J. W. B., Martma, T., Nam, S. & Knies, J. 2019: Discharge of meteoric water in the eastern Norwegian Sea Since the last glacial period. *Geophysical Research Letters 46*, 8194–8204. https://doi.org/10.1029/2019GL084237

Hovland, M. 2002: On the self-sealing nature of marine seeps. *Continental Shelf Research 22*, 2387–2394. https://doi.org/10.1016/S0278-4343(02)00063-8

Hovland, M., Gardner, J. V. & Judd, A. G. 2002: The significance of pockmarks to understanding fluid flow processes and geohazards. *Geofluids 2*, 127–136. https://doi.org/10.1046/j.1468-8123.2002.00028.x

Hustoft, S., Bünz, S., Mienert, J. & Chand, S. 2009: Gas hydrate reservoir and active methane-venting province in sediments on <20 Ma young oceanic crust in the Fram Strait, offshore NW–Svalbard. *Earth and Planetary Science Letters 284*, 12–24. https://doi.org/10.1016/j.epsl.2009.03.038

Jerram, K., Weber, T. C. & Beaudoin, J. 2015: Split-beam echo sounder observations of natural methane seep variability in the northern Gulf of Mexico. *Geochemistry, Geophysics, Geosystems 16*, 736-750. https://doi.org/10.1002/2014GC005429

Johnson, J.E., Mienert, J., Plaza-Faverola, A., Vadakkepuliyambatta, S., Knies, J., Buenz, S., Andreassen, K. & Ferre, B. 2015: Abiotic methane from ultraslow-spreading ridges can charge Arctic gas hydrates. *Geology 43*, 371–374. https://doi.org/10.1130/G36440.1

Jokat, W., Geissler, W. & Voss, M. 2008: Basement structure of the north–western Yermak Plateau. *Geophysical Research Letters 35.* https://doi.org/10.1029/2007GL032892

Jones, A.T, Greinert, J., Bowden, D.A., Klaucke, I., Petersen, C.J., Netzeband, G.L. & Weinrebe, W. 2010: Acoustic and visual characterisation of methane-rich seabed seeps at Omakere Ridge on the Hikurangi Margin, New Zealand. *Marine Geology 272*, 154–169. https://doi.org/10.1016/j.margeo.2009.03.008

Kandilarov, A., Mjelde, R., Okino, K. & Murai, Y. 2008: Crustal structure of the ultra-slow spreading Knipovich Ridge, North Atlantic, along a presumed amagmatic portion of oceanic crustal formation, *Marine Geophysical Research 29*, 109–134. https://doi.org/10.1007/s11001-008-9050-0

Klitzke, P., Franke, D., Ehrhardt, A., Lutz, R., Reinhardt, L., Heyde, I., & Faleide, J. I. 2019: The Paleozoic evolution of the Olga Basin region, northern Barents Sea: A link to the Timanian orogeny. *Geochemistry, Geophysics, Geosystems 20*, 614–629. https://doi.org/10.1029/2018GC007814

Knies, J., Daszinnies, M., Plaza-Faverola, A., Chand, S., Sylta, Ø., Bünz, S., Johnson, J.E., Mattingsdal, R. & Mienert, J. 2018: Modelling persistent methane seepage offshore western Svalbard since early Pleistocene. *Marine and Petroleum Geology 91*, 800–811.
https://doi.org/10.1016/j.marpetgeo.2018.01.020

Kvenvolden, K. A. 1988: Methane hydrate – A major reservoir of carbon in the shallow geosphere? *Chemical Geology 71*, 41–51. https://doi.org/10.1016/0009-2541(88)90104-0

Laberg, J.S. & Vorren, T.O. 1995: Late Weichselian submarine debris flow deposits on the Bear Island Trough Mouth Fan. *Marine Geology 127*, 45–72. https://doi.org/10.1016/0025-3227(95)00055-4

Lasabuda, A.P.E., Johansen, N.S., Laberg, J.S., Faleide, J.I., Senger, K., Rydningen, T.A., Patton, H., Knutsen, S.-M. & Hanssen, A. 2021: Cenozoic uplift and erosion of the Norwegian Barents Shelf – A review. *Earth-Science Reviews 217*, 103609. https://doi.org/10.1016/j.earscirev.2021.103609

Lundschien, B.A., Høy, T. & Mørk, A. 2014: Triassic hydrocarbon potential in the Northern Barents Sea; integrating Svalbard and stratigraphic core data. *NPD Bulletin,* No. 11, pp. 17.

Mattingsdal, R. 2020: Geological controls on widespread gas leakage at the seafloor in the northern Barents Sea. *Abstracts and Proceedings, Geological Society of Norway Annual Meeting, 8–10 January, Oslo, Norway, p. 134.*

Mattingsdal, R., Knies, J., Andreassen, K., Fabian, K., Husum, K., Grøsfjeld, K. & De Schepper, S. 2014: A new 6 Myr stratigraphic framework for the Atlantic–Arctic Gateway. *Quaternary Science Reviews 92,* 170–178. https://doi.org/10.1016/j.quascirev.2013.08.022

Mattingsdal, R., Serov, P., Patton, H., Andreassen, K. & Knutsen, S.-M. 2021: Natural gas seepage from the seafloor above known hydrocarbon discoveries in the southern Barents Sea and the link to the petroleum system. *Abstracts and Proceedings, Geological Society of Norway Annual Meeting, 6–8 January, Oslo, Norway, p. 46.*

Mau, S., Römer, M., Torres, M. E., Bussmann, I., Pape, T., Damm, E., Geprägs, P., Wintersteller, P., Hsu, C. W., Loher, M. & Bohrmann, G. 2017: Widespread methane seepage along the continental margin off Svalbard - from Bjørnøya to Kongsfjorden. *Scientific Reports 7*, 42997.
https://doi.org/10.1038/srep42997

McGinnis, D.F., Greinert, J., Artemov, Y., Beaubien, S.E. & Wuest, A. 2006: Fate of rising methane bubbles in stratified waters: How much methane reaches the atmosphere? *Journal of Geophysical Research 111*, C09007. https://doi.org/10.1029/2005JC003183

Milkov, A.V. 2004: Global estimates of hydrate-bound gas in marine sediments: how much is really out there? *Earth-Science Reviews 66*, 183–197. https://doi.org/10.1016/j.earscirev.2003.11.002

Milkov, A.V. & Sassen, R. 2003: Two-dimensional modeling of gas hydrate decomposition in the northwestern Gulf of Mexico: significance to global change assessment. *Global and Planetary Change 36,* 31–46. https://doi.org/10.1016/S0921-8181(02)00162-5

Müller, R., Nystuen, J. P., & Lie, H. 2005: Late Permian to Triassic basin infill history and palaeogeography of the Mid-Norwegian shelf - East Greenland Region. *In* B.T.G. Wandås, J.P. Nystuen, E. Eide, F. Gradstein (eds.): *Onshore-Offshore Relationships on the North Atlantic Margin*, Norwegian Petroleum Society Special Publications 12, 165–189. https://doi.org/10.1016/S0928-8937(05)80048-7

Müller, R., Klausen, T.G., Faleide, J.I., Olaussen, S., Eide, C.H. & Suslova, A. 2019: Linking regional unconformities in the Barents Sea to compression-induced forebulge uplift at the Triassic–Jurassic transition, *Tectonophysics 765,* 35–51. https://doi.org/10.1016/j.tecto.2019.04.006

Naudts, L., Greinert, J., Artemov, Y., Staelens, P., Poort, J., Van Rensbergen, P. & De Batist, M. 2006: Geological and morphological setting of 2778 methane seeps in the Dnepr paleo-delta, northwestern Black Sea. *Marine Geology 227*, 177–199. https://doi.org/10.1016/j.margeo.2005.10.005

Naudts, L., Greinert, J., Poort, J., Belza, J., Vangampelaere, E., Boone, D., Linke, P., Henriet, J-P. & De Batist, M. 2010: Active venting sites on the gas hydrate bearing Hikurangi Margin, off New Zealand: Diffusive- vs. bubble-released methane. *Marine Geology 272,* 233–250. https://doi.org/10.1016/j.margeo.2009.08.002

Nikolovska, A., Sahling, H. & Bohrmann, G. 2008: Hydroacoustic methodology for detection, localization, and quantification of gas bubbles rising from the seafloor at gas seeps from the eastern Black Sea. *Geochemistry, Geophysics, Geosystems 9*, 13 pp. https://doi.org/10.1029/2008GC002118

Nixon, F.C., Chand, S., Thorsnes, T. & Bjarnadóttir, L.R. 2019: A modified gas hydrate-geomorphological model for a new discovery of enigmatic craters and seabed mounds in the Central Barents Sea, Norway. *Geo-Marine Letters 39*, 191–203. https://doi.org/10.1007/s00367-019-00567-1

NPD 2022. Structural elements of the Norwegian Continental Shelf. http://www.npd.no/en/Topics/Geology/Temaartikler/Structure-elements/ - download 19.01.2022.

Orphan, V.J., Ussler, W., Naehr, T.H., House, C.H., Hinrichs, K.-U. & Paull, C.K. 2004: Geological, geochemical and microbial heterogeneity of the seafloor around methane vents in the Eel River Basin, offshore California. *Chemical Geology 205,* 265–289. https://doi.org/10.1016/j.chemgeo.2003.12.035

Osmundsen, P.T., Sommaruga, A., Skilbrei, J.R. & Olesen, O. 2002: Deep structure of the Mid Norway rifted margin. *Norwegian Journal of Geology 82,* 205–224.

Panieri, G., Bünz, S., Fornari, D.J., Escartin, J., Serov, P., Jansson, P., Torres, M.E., Johnson, J.E., Hong, W., Sauer, S., Garcia, R. & Gracias, N. 2017: An integrated view of the methane system in the pockmarks at Vestnesa Ridge, 79°N. *Marine Geology 390*, 282–300. https://doi.org/10.1016/j.margeo.2017.06.006

Pedersen, R., Thorseth, I., Nygård, T., Lilley, M. & Kelley, D. 2010: Hydrothermal Activity at the Arctic Mid-Ocean Ridges. *Washington DC American Geophysical Union Geophysical Monograph Series 188*, 67–89. https://doi.org/10.1029/2008GM000783

Petersen, T., Thomsen, T., Olaussen, S. & Stemmerik, L. 2016: Provenance shifts in an evolving Eurekan foreland basin: the Tertiary Central Basin, Spitsbergen. *Journal of the Geological Society 173*, 634–638. https://doi.org/10.1144/jgs2015-076

Pohlman, J.W., Bauer, J.E., Canuel, E.A., Grabowski, K.S., Knies, D.L., Mitchell, C.S., Whiticar, M.J. & Coffin, R.B. 2009: Methane sources in gas hydrate-bearing cold seeps: Evidence from radiocarbon and stable isotopes. *Marine Chemistry 115*, 102–109. https://doi.org/10.1016/j.marchem.2009.07.001

Pohlman, J.W., Bauer, J.E., Waite, W.F., Osburn, C.L. & Chapman, N.R. 2011: Methane hydrate-bearing seeps as a source of aged dissolved organic carbon to the oceans. *Nature Geoscience 4*, 37–41. https://doi.org/10.1038/ngeo1016

Rajan, A., Mienert, J., Bünz, S. & Chand, S. 2012: Potential serpentinization, degassing, and gas hydrate formation at a young (<20 Ma) sedimented ocean crust of the Arctic Ocean ridge system. *Journal of Geophysical Research 117*, 14 pp. https://doi.org/10.1029/2011JB008537

Riis, F., Lundschien, B.A., Høy, T., Mørk, A. & Mørk, M.B.E. 2008: Evolution of the Triassic shelf in the northern Barents Sea. *Polar Research 27*, 318–338. https://doi.org/10.1111/j.1751-8369.2008.00086.x

Roy, S., Senger, K., Hovland, M., Römer, M., Braathen, A. 2019: Geological controls on shallow gas distribution and seafloor seepage in an Arctic fjord of Spitsbergen, Norway. *Marine and Petroleum Geology 107*, 237–254. http://dx.doi.org/10.1016/j.marpetgeo.2019.05.021

Ryseth, A., Augustson, J.H., Charnock, M., Haugerud, O., Knutsen, S.-M., Midbøe, P.S., Opsal, J.G. & Sundsbø, G. 2003: Cenozoic stratigraphy and evolution of the Sørvestsnaget Basin, southwestern Barents Sea. *Norwegian Journal of Geology 83*, 107–130.

Sassen, R., Joye, S., Sweet, S.T., DeFreitas, D.A., Milkov, A.V. & MacDonald, I.R. 1999: Thermogenic gas hydrates and hydrocarbon gases in complex chemosynthetic communities, Gulf of Mexico continental slope. *Organic Geochemistry 30*, 485–497. https://doi.org/10.1016/S0146-6380(99)00050-9

Schneider von Deimling, J., Brockhoff, J. & Greinert, J. 2007: Flare imaging with multibeam systems: Data processing for bubble detection at seeps. *Geochemistry, Geophysics, Geosystems 8*, Q06004. https://doi.org/10.1029/2007GC001577 https://doi.org/10.1038/ngeo2232

Serov, P., Mattingsdal, R., Winsborrow, M., Patton, H. & Andreassen, K. 2023: Widespread natural methane and oil leakage from sub-marine Arctic reservoirs. *Nature Communications 14*, 1782. https://doi.org/10.1038/s41467-023-37514-9

Sigmond, E.M.O. 2002. Geological map, Land and Sea areas of Northern Europe. Scale 1:4 million. *Geological Survey of Norway.*

Skarke, A., Ruppel, C., Kodis, M., Brothers, D., & Lobecker, E. 2014: Widespread methane leakage from the sea floor on the northern US Atlantic margin. *Nature Geoscience 7*, 657-661. https://doi.org/10.1038/ngeo2232

Suess, E. 2014: Marine cold seeps and their manifestations: geological control, biogeochemical criteria and environmental conditions. *International Journal of Earth Sciences 103*, 1889–1916. https://doi.org/10.1007/s00531-014-1010-0

Thorsnes, T., Chand, S., Brunstad, H., Lepland, A. & Lågstad, P. 2019: Strategy for Detection and High-Resolution Characterization of Authigenic Carbonate Cold Seep Habitats Using Ships and Autonomous Underwater Vehicles on Glacially Influenced Terrain. *Frontiers in Marine Science 6.* https://doi.org/10.3389/fmars.2019.00708

Thorsnes, T., Misund, O. A., & Smelror, M. 2020: Seabed mapping in Norwegian waters: programmes, technologies and future advances. *In* Hill, P. R., Lebel, D., Hitzman, M., Smelror, M. & Thorleifson, H. (eds.): *The Changing Role of Geological Surveys*. Geological Society, London, Special Publications, 49. https://doi.org/10.1144/SP499-2019-69

Tsikalas, F., Faleide, J.I. & Kusznir, N.J. 2008: Along-strike variations in rifted margin crustal architecture and lithosphere thinning between northern Vøring and Lofoten margin segments off mid–Norway. *Tectonophysics 458,* 68–81. https://doi.org/10.1016/j.tecto.2008.03.001

Tucholke, B.E., Lin, J. & Kleinrock, M.C., 1998: Megamullions and mullion structure defining oceanic metamorphic core complexes on the Mid-Atlantic Ridge. *Journal of Geophysical Research 103*, 9857–9866. https://doi.org/10.1029/98JB00167

Uchimoto, K., Nishimura, M. Watanabe, Y. & Xue, Z. 2019: Bubble Detection with Side-scan Sonar in Shallow Sea for Future Application to Marine Monitoring at Offshore CO_2 storage sites. *American Journal of Marine Science 7*, 1–6.

Vorren, T., Lebesbye, E., Andreassen, K. & Larsen, K.-B. 1989: Glacigenic sediments on a passive continental margin as exemplified by the Barents Sea. *Marine Geology 85*, 251–272. https://doi.org/10.1016/0025-3227(89)90156-4

Vorren, T.O., Richardsen, G., Knutsen, S.-M. & Henriksen, E. 1991: Cenozoic erosion and sedimentation in the western Barents Sea. *Marine and Petroleum Geology 8*, 317–340. https://doi.org/10.1016/0264-8172(91)90086-G

Vorren, T., Laberg, J. S., Blaume, F., Dowdeswell, J. A., Kenyon, N. H., Mienert, J., Rumohr, J. & Werner, F. 1998: The Norwegian¬–Greenland Sea Continental Margins: Morphology and Late Quaternary sedimentary Processes and Environment. *Quaternary Science Reviews 17*, 273–302. https://doi.org/10.1016/S0277-3791(97)00072-3

Waage, M., Portnov, A., Serov, P., Bünz, S., Waghorn, K. A., Vadakkepuliyambatta, S., Mienert, J., & Andreassen, K. 2019: Geological controls on fluid flow and gas hydrate pingo development on the Barents Sea margin. *Geochemistry, Geophysics, Geosystems 20,* 630–650. https://doi.org/10.1029/2018GC007930

Waage, M., Serov, P., Andreassen, K., Waghorn, K.A., & Bünz, S. 2020: Geological controls of giant crater development on the Arctic seafloor. *Scientific Reports 10*, 8450. https://doi.org/10.1038/s41598-020-65018-9

Weber, T. C., Mayer, L., Jerram, K., Beaudoin, J., Rzhanov, Y. & Lovalvo, D. 2014: Acoustic estimates of methane gas flux from the seabed in a 6000 km^2 region in the Northern Gulf of Mexico. *Geochemistry, Geophysics, Geosystems 15*, 1911–1925. https://doi.org/10.1002/2014GC005271

Westbrook, G.K., Chand, S., Rossi, G., Long, C., Bünz, S., Camerlenghi, A., Carcione, J.M., Dean, S., Foucher, J.-P., Flueh, E., Gei, D., Haacke, R.R., Madrussani, G., Mienert, J., Minshull, T.A., Nouzé, H., Peacock, S., Reston, T.J., Vanneste, M. & Zillmer, M. 2008: Estimation of gas hydrate concentration from multi-component seismic data on the continental margins of NW Svalbard and the Storegga region of Norway. *Marine and Petroleum Geology 25*, 744–758. https://doi.org/10.1016/j.marpetgeo.2008.02.003

Westbrook, G.K., Thatcher, K.E., Rohling, E.J., Piotrowski, A.M., Palike, H., Osborne, A.H., Nisbet, E.G., Minshull, T.A., Lanoiselle, M., James, R.H., Huhnerbach, V., Green, D., Fisher, R.E., Crocker, A.J., Chabert, A., Bolton, C., Beszczynska-Moller, A., Berndt, C. & Aquilina, A. 2009: Escape of methane gas from the seabed along the West Spitsbergen continental margin. *Geophysical Research Letters 36,* 5 pp. https://doi.org/10.1029/2009GL039191

Wilpshaar, M., de Bruin, G., Versteijlen, N., van der Valk, K. & Griffioen, J. 2021: Comment on "Greenhouse gas emissions from marine decommissioned hydrocarbon wells: Leakage detection, monitoring and mitigation strategies" by Christoph Böttner, Matthias Haeckel, Mark Schmidt, Christian Berndt, Lisa Vielstädte, Jakob A. Kutsch, Jens Karstens & Tim Weiß. *International Journal of Greenhouse Gas Control 110,* 103395. https://doi.org/10.1016/j.ijggc.2021.103395.

Åstrøm, E.K.L., Carroll, M.L., Ambrose, W.G., Sen, A., Silyakova, A. & Carroll, J. 2018: Methane cold seeps as biological oases in the high-Arctic deep sea. *Limnology and Oceanography 63*, 209–231. https://doi.org/10.1002/lno.10732